2016

Development of Protein-Polymer Core-Shell Nanoparticles (PPCS-NPs) as Efficient Vehicles to Deliver Therapeutic Agents Across Blood Brain Barrier (BBB)

Napat Tandikul
University of South Carolina

Development of Protein-Polymer Core-Shell Nanoparticles (PPCS-NPs) as efficient vehicles to deliver therapeutic agents across Blood Brain Barrier (BBB)

by

Napat Tandikul

Bachelor of Science
Chulalongkorn University, 2011

Submitted in Partial Fulfillment of the Requirements

For the Degree of Master of Science in

Chemistry

College of Arts and Sciences

University of South Carolina

2016

Accepted by:

Qian Wang, Director of Thesis

Thomas M. Makris, Reader

Lacy Ford, Senior Vice Provost and Dean of Graduate Studies

DEDICATION

I would like to dedicate this thesis…

To my mom, my dad and my brother for all their forever love, care and support,

To Mae Noon, who is suffering from Her2 positive breast cancer that is now penetrating her brain and Nong Einz, who passed away from Ependymoblastoma for the inspiration that encourages me to work on this research.

ACKNOWLEDGEMENTS

First and foremost, I would like to thank Dr. Qian Wang for giving me a great opportunity to join his research group and thank you for all his generous help during these two and a half years at the University of South Carolina. I would also like to thank Dr. Thomas Makris, Dr. Chuanbing Tang and Dr. Michael Wyatt for their suggestions for my research plan and special thanks to Dr. Makris for always willing to help and for being my thesis reader.

Thank you to all the members in Dr. Wang's research group for sharing memories together, especially, Dr. Gary Horvath for training me well since the first day I joined this lab; Dr. Yuzhe Nie and Dr. Xiaolei Zhang for their help in MALDI-MS and peptide analysis; and Dr. Jing Yan for providing me with a basic introduction to polymer and self-assembly technique and for synthesizing PCL-py polymer.

I would like to also gratefully thank my former advisors, Dr.Weerapong Prasongchean for his training and advice before and during my graduate study life, Dr.Pakorn Winayanuwattikun, and Assoc. Prof. Dr. Vichien Rimphanitchayakit for their support in the admission process to University of South Carolina. Thank you Dr. Nitsara Karoonuthaisiri for being my role model, my inspiration, my forever favorite woman scientist and my long-lost sister, thank you for all her suggestions, comments and support. She always make me calm down and stay positive about my poor graduate student life.

Thank you all professors at the University of South Carolina, especially Dr. Amy Taylor-Perry for being my role model of a good “teacher”. I thank all my friends at the University of South Carolina. I could not believe that I have friends from all around the world. Thank you Malini, TT, John, Nikita, Evan and Safaa for their friendships and for being so supportive and always listen to me when I have tough time. Special thanks to Gift, Amie and Nikki for helping me settling down when I first moved to Columbia and for their general advices.

Thank you my host family, Mr.Paul Rouppasong and Na Malivan for spoiling me with good food and always providing me kindness and generosity. Of course, thank you my long-lost sister, Nong Sala Dang, who brings laugh and happiness to my graduate life, and take me to everywhere I want. I also thank Kevin, Blair, Briana, Eli and P’Bung for spending good times and sharing good memories at Rouppasong’s house. I also thank Pa Sri who taking good care of me, and sending me food and love even though we are far apart. I thank P’Oa, my graduate student 101 teacher, who always shares her experiences and gives me clear answers for all my questions about my poor graduate study life and all her support.

Finally and most importantly, I would like to thank my parents, Mr. Piroj and Mrs. Yanaporn Tandikul and my brother, for their faith in my dream, for rooting me with love, support, patience and understanding throughout my life. I would not have made it today without them. I would also like to thank my best friends, the gang, in Thailand, Patt, Ploy, Nat, June, for their care and supports even if we are 9,144 miles apart. Our 10 years of friendship will last forever. Special thanks to Nisachon, my best friend who always stands by me even in the darkest day of my life.

Last but not least, thank you for all obstacles throughout my graduate life that make me stronger, just like J.K.Rowling said “Rock bottom became the solid foundation on which I rebuilt my life.

ABSTRACT

Blood Brain Barrier (BBB) plays a main role as selective barrier which controls and limits access of chemicals, molecules and therapeutic agents from blood to brain. The BBB endothelial cells are connected by Tight Junctions (TJs) which close intracellular spaces between the endothelial cells and block the free diffusion of substances, therefore many potential drugs for treating human brain diseases cannot reach the brain in sufficient concentration. Recently, many studies have thrown an interest in development of nanoparticles for delivering drugs and imaging agents across BBB. Our research group has developed protein-polymer core-shell nanoparticles (PPCS-NPs) which demonstrate great potential for targeted delivery. In this work, Apolipoprotein E3 (ApoE3), which can be specifically bound to LDLR receptor on BBB endothelial cells, was chosen as a targeted motif. Nanoparticles conjugated with ApoE3 and fluorescently labelled ApoE3 (Fl-ApoE3) were successfully synthesized. The synthesis of ApoE3/ Fl-ApoE3 NPs with encapsulation of drugs and dyes is in progress. In vitro study of the uptake of ApoE3-NPs, Fl-ApoE3-NPs with and without encapsulation of drugs and dyes will be further investigated by using human umbilical vein endothelial cells (HUVECs) and brain microvascular endothelial cell line (hCMEC/D3) as BBB endothelial cell model.

TABLE OF CONTENTS

DEDICATION iii

ACKNOWLEDGEMENTS iv

ABSTRACT vii

LIST OF TABLES x

LIST OF FIGURES xi

CHAPTER 1: BACKGROUND AND SIGNIFICANCE 1

1.1 INTRODUCTION 1

1.2 BLOOD BRAIN BARRIER (BBB) 1

1.3 NANOPARTICLE FOR DRUG DELIVERY 5

1.4 NANOPARTICLES UPTAKE AND TRANSPORT ACROSS BBB 7

1.5 STATEMENT OF WORK 9

REFERENCES 10

CHAPTER 2: PURIFIACATION OF APOLIPOPROTEIN E AND SYNTHESIS OF FLUORESCENTLY LABELLED APOE3 (FL-APOE3) 13

2.1 APOLIPOPROTEIN E 13

2.2 PURIFICATION AND ANALYSIS OF APOLIPOPROTIEN E3, E4 16

2.3 SYNTHESIS OF FLUORESCENTLY LABELLED APOE3 (FL-APOE3) 20

2.4 CONCLUSION 22

2.5 MATERIALS AND METHOD 23

REFERENCES 27

CHAPTER 3: SELF-ASSEMBLY AND CELL UPTAKE OF PROTEIN POLYMER CORE SHELL NANOPARTICLES 28

3.1 INTRODUCTION....28

3.2 SELF-ASSEMBLY OF APOE3-P4VP NANOPARTICLES (APOE3-P4VP-NPS)....31

3.3 SELF-ASSEMBLY OF FLUORESCENTLY LABELLED APOE3-P4VP NANOPARTICLES (FL-APOE3-P4VP-NPS) 33

3.4SELF-ASSEMBLY OF APOE3-P4VP NANOPARTICLES (APOE3-PCL-PY-NPS) 35

3.5 CELL VIABILITY ASSAY....37

3.6 NANOPARTICLES UPTAKE HUVECS AND HMSCS....39

3.7 SELF-ASSEMBLY OF FLUORESCENTLY LABELED APOE3-P4VP ENCAPSULATED NILE RED NANOPARTICLES (FL-APOE3-P4VP/NR-NPS)....44

3.8 CONCLUSION 45

3.9 MATERIALS AND METHOD 45

REFERENCES 50

LIST OF TABLES

Table 2.1 Prevalence of the human ApoE isoforms and their key differences. Adapted with permission from Hatter, D.M. *et al* (2006) *Trends Biochem Sci*, 31, 445-454.....15

Table 3.1 Sizes of ApoE3-P4VP-NPs measured by DLS (a-c) with different mass ratios of proteins to P4VP (M_{ApoE3}/M_{P4VP}). 33

Table 3.2 Sizes of Fl-ApoE3-P4VP-NPs measured by DLS (a-c) with different mass ratios of proteins to P4VP ($M_{Fl\text{-}ApoE3}/M_{P4VP}$). 34

Table 3.3 Sizes of ApoE3-PCL-py-NPs measured by DLS (a-c) with different mass ratios of proteins to PCL-py ($M_{ApoE3}/M_{PCL\text{-}py}$).....37

Table 3.4 Sizes of Fl-ApoE3-P4VP/NR-NPs measured by DLS (a-c) with different mass ratios of proteins to P4VP/NR ($M_{Fl\text{-}ApoE3}/M_{P4VP/NR}$). 44

LIST OF FIGURES

Figure 1.1 Blood Brain Barrier and cell association overview (top). The cell association at the BBB (bottom). The cerebral endothelial cells form tight junctions at the margins (bottom, red circle) which block the aqueous paracellular diffusional pathway. Pericytes which distribute along the endothelial cells ensheath the endothelium and contribute to the local basement membrane which forms basal lamina. Astrocytic endfeet of the astrocytes form a complex network and cell association around the capillaries which help in maintenance of the BBB properties. Microglia, which are the resident of immunocompetent cells, regulate BBB properties during embryogenesis and disease. Figure is adapted with permission from Abbott, N.J. *et al.* (2010) Structure and function of the blood-brain barrier. *Neurobio Dis*. 37(1), 13-25. 2

Figure 1.2 Mechanism and different pathways for molecules across BBB. **a)** Paracellular pathway for water soluble molecules, the molecules were blocked by tight junction (TJs). **b)** Transcellular lipophilic pathway for lipid-soluble molecules. **c)** Carrier-mediated transport as occurs for glucose, amino acids, nucleosides, etc. **d)** Efflux pump, molecules can be pumped out by transporters on endothelial cell membrane. **e)** Receptor mediated transcytosis for peptide signaling and regulatory molecules, e.g. insulin, transferrin. **f)** Adsorptive transcytosis for positively charged cargo (serum proteins) transport. Figure is adapted with permission from Chen, Y. and Liu, L. (2012) Structure and function of the blood–brain barrier. *Adv Drug Deliv Rev* 64 (7), 640-665. 4

Figure 1.3 Example of nanocarriers (adapted with permission from Dan, P. *et al*. (2007) *Nature Nanotechnology* 2, 751 – 760) 6

Figure 2.1 ApoE3 has two structural domains, N-terminal domain (red) which contains receptor binding region and C-terminal domain (blue) which contains lipid binding region. Those two domains are linked by hinge region (gray). ApoE2, E3 and E4 isoforms are encoded by the ε2, ε3 and ε4 alleles on ApoE gene respectively. There are two polymorphic positions, 112 and 158, that distinguish the three common isoforms. Figure is adapted with permission from Liu, C-C. *et al* (2013) *Nat Rev Neurol*, 9, 106-118. **b)** The model structure illustrating the full length human ApoE3 created by Chen, J. *et al* (2011) *Proc. Natl. Acad. Sci,* 108, p.14813. Solution NMR method was used in studying the structure of the ApoE3 and the picture was produced by PyMOL. **c)** Model of the structure of ApoE3 and ApoE4 and structural difference of ApoE3 and ApoE4. Key structural elements of ApoE are N-terminal domain which contains a four helix bundle (helix1, red; helix2, blue; helix3, green; helix4, yellow) and C-terminal domain (gray) which contains lipid binding elements. Main differences is a putative salt bridge between Arg-61 and Glu-255 presenting only in ApoE4 that stabilizes a closer contact between the N- and C- terminal domains. Figure is adapted with permission from Hatter, D.M. *et al* (2006) *Trends Biochem Sci*, 31, 445-454. 14

Figure 2.2 **a)** SDS-PAGE analysis of the purified ApoE3. Protein were analyzed on a gradient (4-20%) gel and stained with Coomassie blue. Lane 1, ApoE3 with a concentration of 2.52 µg/mL; lane 2, ApoE3 with a concentration of 4.00 µg/mL; Lane 3, ApoE3 with a concentration of 6.00 µg/mL. The molecular weight of ApoE3 was a little higher than 34.0 kDa (Red arrow). **b)** Western blot analysis of purified ApoE3 against 1^{o} antibody, Goat anti human ApoE, and 2^{o} antibody, Fab anti-goat IgG (Donkey antibody), shown ApoE expression at molecular weight of about 34 kDa. Lane 1-5 was ApoE3 with a concentration of 2.0, 4.0, 6.0, 8.0, 10.0 ng/mL. **c)** MALDI-MS analysis of purified ApoE3 showed the molecular mass of unmodified ApoE3 as 35,085.56 m/z (red arrow). **d)** Peptide analysis peak list of ApoE3 created by FlexAnalysis software. **e)** Peptide analysis by MASCOT software, identical residues were highlighted in red with 62% recovery and MASCOT score of 75. 18

Figure 2.3 ApoE4 determination by SDS-PAGE. Protein were analyzed on a gradient (4-20%) gel and stained with Coomassie blue. Lane 1, ApoE4 with a concentration of 2.5 µg/mL; Lane 2, ApoE4 with a concentration of 5.0 µg/mL; Lane 3, ApoE4 with a concentration of 9.90 µg/mL. The result showed a lot of impurities indicated that the purification process was not successfully done. 20

Figure 2.4 Schematic illustration of the synthesis of Fl-ApoE3 20

Figure 2.5 Fl**-**ApoE3 identification by SDS-PAGE visualized under EPI white (left) and UV-VIS (right). Fluorescent signal can only be seen in the lane loaded with Fl-ApoE3. The molecular mass of Fl-ApoE3 was approximately about 34 kDa. 21

Figure 2.6 MALDI-MS analysis of Fl-ApoE3 showed the molecular mass of Fl-ApoE3 was 35,128.53 m/z (red arrow). 22

Figure 3.1 Schematic illustration of the formation of Fl-ApoE3 nanoparticles (Fl-ApoE3 NPs) and the study of nanoparticles uptake in HUVECs cells. 30

Figure 3.2 **(a)** Schematic illustration of the synthesis of ApoE3-P4VP-NPs. **(b)** DLS results of ApoE3-P4VP-NPs with different mass ratio (M_{ApoE3}/M_{P4VP}): 0.60, 1.20 and 2.40. TEM images of ApoE3-P4VP-NPs at different mass ratio, where **(c)** M_{ApoE3}/M_{P4VP} = 0.60, **(d)** M_{ApoE3}/M_{P4VP} = 1.20, and **(e)** M_{ApoE3}/M_{P4VP} = 2.40. **(f)** Circular dichroism of ApoE3 and ApoE3-P4VP-NPs. ApoE3:P4VP-a: M_{ApoE3}/M_{P4VP} = 0.60; ApoE3:P4VP-b: M_{ApoE3}/M_{P4VP} = 1.20; and ApoE3:P4VP-c: M_{ApoE3}/M_{P4VP} = 2.40. Both native ApoE3 and ApoE3-P4VP-NPs does not clearly show two minima at 208 (1) and 222 (2) nm. 31

Figure 3.3 **(a)** Schematic illustration of the synthesis of Fl-ApoE3-P4VP-NPs. **(b)** DLS results of Fl-ApoE3-P4VP-NPs with different mass ratio ($M_{Fl\text{-}ApoE3}/M_{P4VP}$: 0.60, 1.20 and 2.40). TEM images of Fl-ApoE3-P4VP-NPs at different mass ratio, where **(c)** $M_{Fl\text{-}ApoE3}/M_{P4VP}$ = 0.60 **(d)** $M_{Fl\text{-}ApoE3}/M_{P4VP}$ = 1.20 **(e)** $M_{Fl\text{-}ApoE3}/M_{P4VP}$ = 2.40. 33

Figure 3.4 **(a)** Schematic illustration of the synthesis of ApoE3-PCL-py-NPs. **(b)** DLS results of ApoE3-PCL-py-NPs with different mass ratio ($M_{ApoE3}/M_{PCL\text{-}py}$) of 0.60, 1.20 and 2.40. TEM images of ApoE3-PCL-py-NPs at different mass ratio, where **(c)** $M_{ApoE3}/M_{PCL\text{-}py}$= 0.60 **(d)** $M_{ApoE3}/M_{PCL\text{-}py}$ = 1.20 **(e)** $M_{ApoE3}/M_{PCL\text{-}py}$ = 2.40. **(f)** Circular dichroism of

ApoE3 and ApoE3-PCL-py-NPs, ApoE3:PCL-py-a is M_{ApoE3}/M_{PCL-py} = 0.60; ApoE3:PCL-py-b is M_{ApoE3}/M_{PCL-py} = 1.20; ApoE3:PCL-py-c is M_{ApoE3}/M_{PCL-py} = 2.40. The CD spectra is not good enough to tell any conformational changes.....35

Figure 3.5 Cell viability assay of (a) ApoE3-P4VP-NPs (b) ApoE3-PCL-py-NPs treated for 24 h.....38

Figure 3.6 Fluorescent microscopic images of HUVECs (LDLR receptor+) cells incubated with Fl-ApoE3, Fl-ApoE3-P4VP-NPs, Fl-BSA-P4VP-NPs for 2, 24h and pre-treated with ApoE3 for 2 h follow by the incubation of Fl-ApoE3-P4VP-NPs for 2, 24 h. The blue nuclei of cells were stained with DAPI. The green fluorescence belonged to the Fl-ApoE3. The scale bars are 20 μm. 40

Figure 3.7 High magnification fluorescent microscopic images of HUVECs (LDLR receptor+) cells incubated with Fl-ApoE3-P4VP-NPs, for 2, 24h. The blue nuclei of cells were stained with DAPI. The green fluorescence belonged to the Fl-ApoE3. The scale bars are 20 μm. 41

Figure 3.8 Fluorescent microscopic images of HUVECs (LDLR receptor+) cells pre-incubated with ApoE3 for 2 h, then incubated with Fl-ApoE3-P4VP-NPs for 2, 24h. The blue nuclei of cells were stained with DAPI. The green fluorescence belonged to the Fl-ApoE3. The scale bars are 20 μm. 42

Figure 3.9 Fluorescent microscopic images of hMSCs (LDLR receptor-) cells incubated with Fl-ApoE3, Fl-ApoE3-P4VP-NPs, Fl-BSA-P4VP-NPs for 2, 24h and pre-treated with ApoE3 for 2 h follow by the incubation of Fl-ApoE3-P4VP-NPs for 2, 24 h. The blue nuclei of cells were stained with DAPI. The green fluorescence belonged to the Fl-ApoE3. The scale bars are 20 μm. 43

Figure 3.10 DLS results of Fl-ApoE3-P4VP/NR-NPs with different mass ratio ($M_{Fl-ApoE3}/M_{P4VP/NR}$) of 0.60, 1.20 and 2.40. 44

CHAPTER 1

BACKGROUND AND SIGNIFICANCE

1.1 INTRODUCTION

In 2010, statistics from American Brain Tumor Association (ABTA) showed that 688,096 Americans were living with the diagnostic of a primary brain tumor. However, Only 0.2% are living after diagnosis (America Brain Tumor Association, 2013). One in nine older Americans, estimated 5.2 million Americans of all ages have Alzheimer's disease. Every year, approximately 150 billion US dollars have been paid for health care and long term care (Alzheimer's Association, 2014). Parkinson's disease foundation reports in 2014 that 1 million Americans are living with Parkinson's disease, and 25 billion US dollars have been paid for treatment in USA each year. One of the crucial problems of human brain diseases treatment is the incapability in efficiently transporting drugs to the brain because of the blood brain barrier.

1.2 BLOOD BRAIN BARRIER (BBB)

Blood brain barrier (BBB) is a selective barrier formed by the endothelial cells that safeguard cerebral microvessels [1, 2]. BBB is the largest surface area for exchanging substances between blood and brain, it is approximately 12-18 m^2 in surface area [3]. Once the BBB is crossed, diffusion distances to neurons and glial cell bodies for solutes and drugs are short [3]. It also protects neurons from systematically circulating potentially

cytotoxic agents by forming a very tight barrier called tight junctions (TJs) [3]. A diffusion barrier, formed by TJs which present between cerebral endothelial cells, severely restrict penetration of water soluble compounds and polar drugs into the brain [3]. The presence of TJs divides plasma membrane of the vascular endothelial cells into two separate domains, apical membrane which faces the blood, and basolateral membrane which faces the brain tissue [4].

STRUCTURE OF BLOOD BRAIN BARRIER

The cell association at the BBB including endothelial cells, basal lamina, astrocytes, pericytes and microglia [4, 5]. Astrocytic end-feet, cover more than 90% of the endothelial cell surface, tightly ensheaths the vessel wall and takes part in the induction, maintenance and robustness of the integrity of endothelial barrier [4, 5]. Astrocytes are important in induction and maintenance of the barrier properties [3]. Pericytes are contractile cells that embrace brain capillary and contributes to the development, maintenance and regulation of BBB [5]. Microglia play a role in regulating BBB properties during embryogenesis and disease (Figure 1.1).

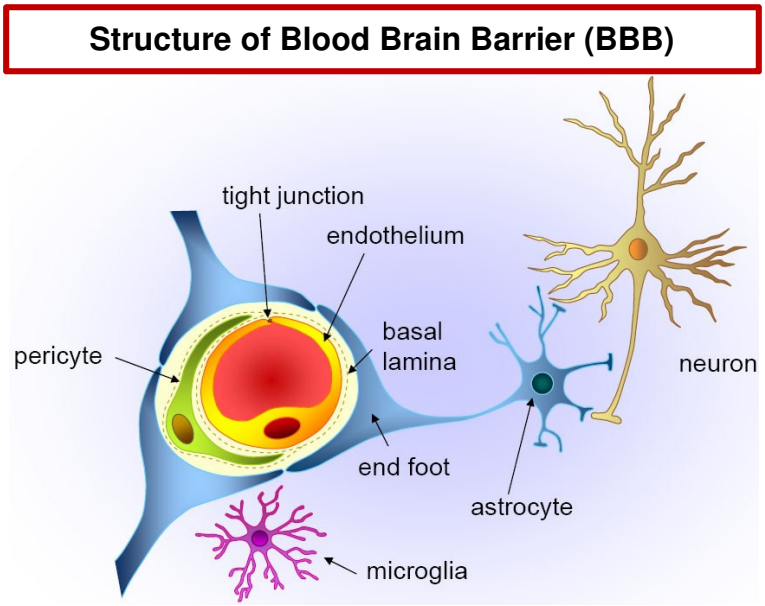

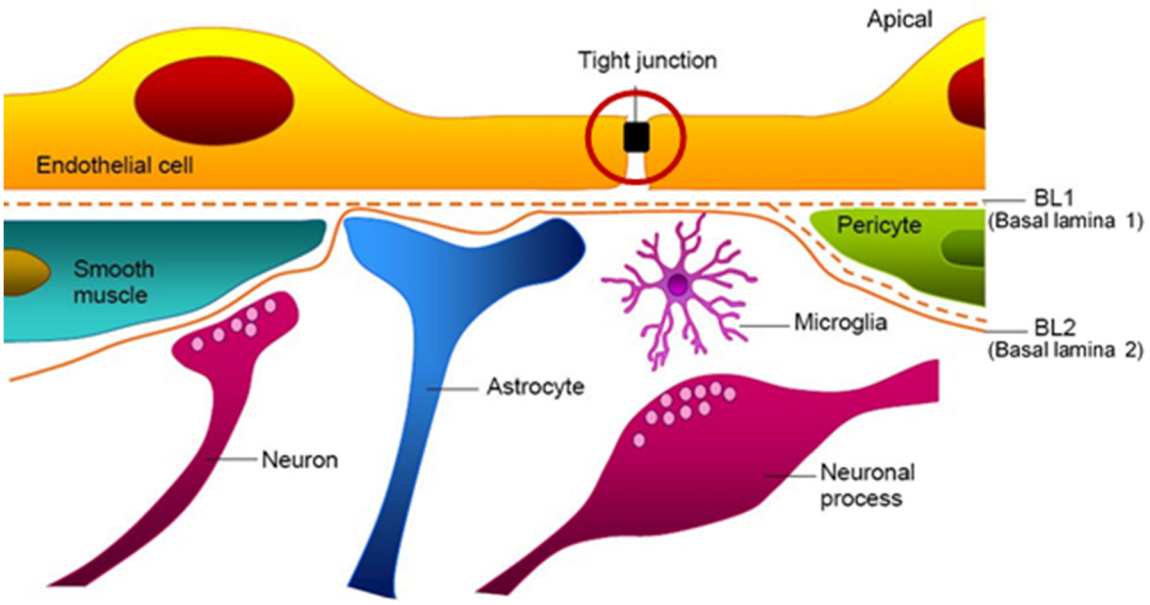

Figure 1.1. Blood Brain Barrier and cell association overview (top). The cell association at the BBB (bottom). The cerebral endothelial cells form tight junctions at the margins (bottom, red circle) which block the aqueous paracellular diffusional pathway. Pericytes which distribute along the endothelial cells ensheath the endothelium and contribute to the local basement membrane which forms basal lamina. Astrocytic endfeet of the astrocytes form a complex network and cell association around the capillaries which help in maintenance of the BBB properties. Microglia, which are the resident of immunocompetent cells, regulate BBB properties during embryogenesis and disease. Figure is adapted with permission from Abbott, N.J. *et al.* (2010) Structure and function of the blood-brain barrier. *Neurobio Dis*. 37(1), 13-25.

Transport across the BBB

Normally, the TJs severely restrict penetration of water-soluble compounds, including polar drugs by regulating paracellular flux [1, 3]. Water soluble or polar compounds can penetrate only by paracellular transport which is limited to small hydrophilic molecules [4, 5]. Lipid-soluble agents (smaller than 400 Da) can effectively diffuse through the large surface area of the lipid membranes of the endothelial cells via transcellular lipophilic pathway [6]. This process is driven by concentration gradient and limited to small hydrophobic molecules [4]. Moreover, it is a main entry route to the brain of current therapeutics [4]. Transportation of glucose, amino acids, purine bases,

nucleosides, choline or other substances require the transporters as specific carriers [1, 4]. However, some transport proteins, such as P-glycoprotein (P-gp), localized on the apical (luminal) side of the brain capillary endothelium, act as efflux transporters and restrict the uptake of drugs into the brain [7]. Additionally, certain proteins, such as insulin and transferrin, are taken up by specific receptor-mediated endocytosis, delivered through BBB by transcytosis and exposed out of the cells by exocytosis [1, 5]. Adsorptive transcytosis relies on transport of positively charged cargo in a non-specific manner [4] (Figure 1.2).

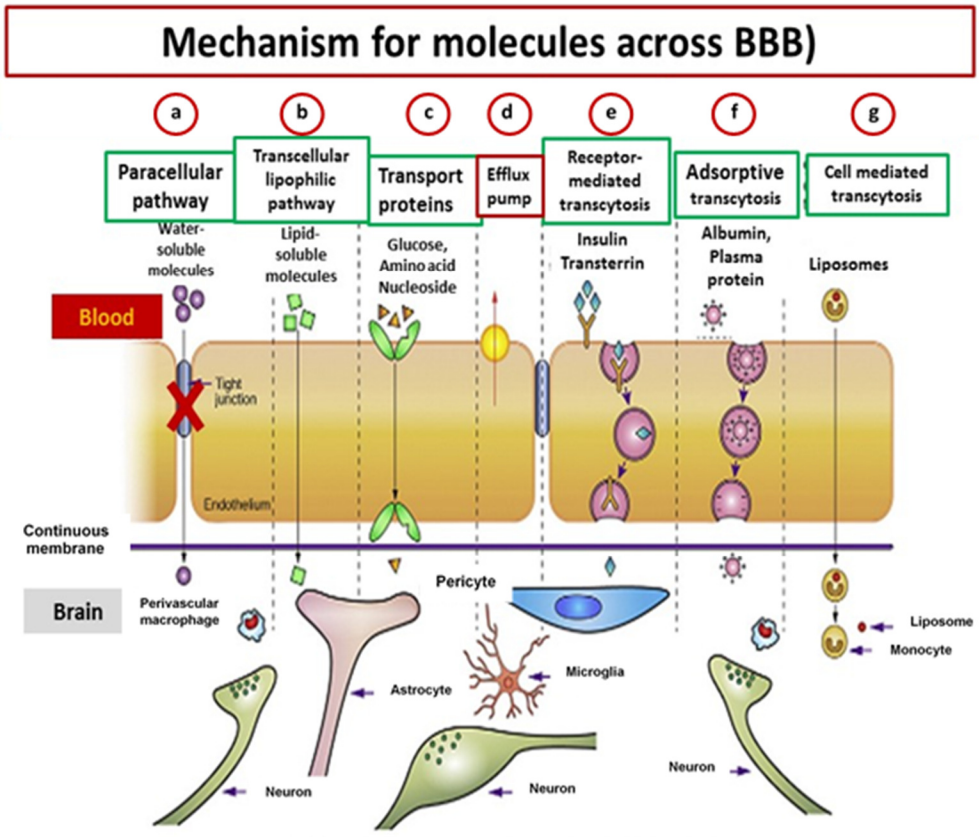

Figure 1.2. Mechanism and different pathways for molecules across BBB. **a)** Paracellular pathway for water soluble molecules, the molecules were blocked by tight junction (TJs). **b)** Transcellular lipophilic pathway for lipid-soluble molecules. **c)** Carrier-mediated transport as occurs for glucose, amino acids, nucleosides, etc. **d)** Efflux pump, molecules can be pumped out by transporters on endothelial cell membrane. **e)** Receptor mediated transcytosis for peptide signaling and regulatory molecules, e.g. insulin, transferrin. **f)** Adsorptive transcytosis for positively charged cargo (serum proteins) transport. Figure is adapted with permission from Chen, Y. and Liu, L. (2012) Structure and function of the blood–brain barrier. *Adv Drug Deliv Rev* 64 (7), 640-665.

1.3 NANOPARTICLES FOR DRUG DELIVERY

A critical problem in the treatment of brain tumor and neurodegenerative diseases such as Alzheimer's disease and Parkinson's disease is the incapability of drugs to be delivered across BBB in the brain [8]. To overcome this problem, many studies have shown an interest in the development of nanoparticles as promising drug delivery agents that can be transported across BBB and increase the uptake of appropriate drugs in the brain [8-12]. The development of nanocarrier-drug system as Trojan horse complex is one of a promising drug targeting technology [4]. From this concept, natural or genetically engineered proteins or small peptides conjugated with appropriate nanocarriers can specifically transport a drug-payload which is directly coupled or encapsulated in the nanocarriers [4]. The important advantages of therapeutic nanoparticles over free drugs are the ability to: 1) prolong blood circulation; 2) control the bio-distribution and release of drugs; 3) site-specific targeting; 4) stabilize labile molecules (e.g. protein, peptides, DNA) on the particles' surface from degradation; and 5) protect a drug from degradation [8, 13, 14]. Moreover, they can be modified to deliver a variety of drugs with improved delivery efficiency and reduced side effects by targeted delivery [8].

DEFINITION OF NANOPARTICLES

The definition of nanoparticles in the Encyclopedia of Pharmaceutical Technology and the Encyclopedia of Nanoscience and Nanotechnology is

"Nanoparticles for pharmaceutical purposes are solid colloidal particles ranging in size from 1 to 1000 nm (1 μm) consisting of macromolecular materials in which the active principle (drug or biologically active material) is dissolved, entrapped, or encapsulated, or to which principle is adsorbed or attached."

On the other side, physicists and material scientists limit the size of nanoparticles not to exceed 100 nm [15]. The definition from NNI (National Nanotechnology Initiative) is "Nanoparticles are structure of sizes ranging from 1 to 100 nm in at least one dimension"[14]. The size above 1000 nm shows no significant influence in cell uptake and may lead to embolization in lung capillaries [15, 16].

TYPES OF NANOPARTICLES

Nanocarriers in medical applications should be **biocompatible** (able to migrate with a biological system without eliciting immune response or any negative effects), and **nontoxic** (harmless to the given biological system) [14]. However, many types of nanoparticles are either toxic or have undesirable effects to cells depending on their hydrodynamic size, shape, amount, surface chemistry, route of administration, response of the immune system, and resident time in blood stream [14]. There are several major types of nanoparticle that have been widely used for development of nanomedicines, including liposomes, dendrimers, polymeric micelles, polymeric carriers that made of biodegradable polymers such as poly(butyl cyanoacrylate) (PBCA), poly(isohexyl cyanoacrelate) (PIHCA), poly(lactic acid) (PLA), poly(lactide-co-glycolide) (PLGA), human serum albumin (HSA), as well as chitosan [17-19], and inorganic carriers such as gold nanoparticles, quantum dot etc.

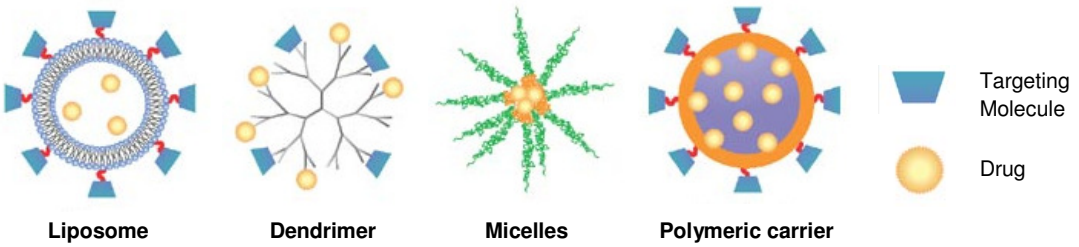

Figure 1.3. Example of nanocarriers (adapted with permission from Dan, P. *et al*. (2007) *Nature Nanotechnology* 2, 751 – 760).

1.4 NANOPARTICLES UPTAKE AND TRANSPORT ACROSS BBB

There are eight possible mechanisms of nanoparticles uptake and of bound drugs into the brain: [16, 20, 21]

1) An increase in retention time of nanoparticles in blood that would lead to higher concentration gradient, and as a result, enhance the delivery to the brain. However, drugs can be subjected to and pumped out by the highly efficient efflux transporters such as P-gp. Thus, the concentration of drug in the brain does not achieve pharmacological effects.

2) Surfactant or coating agents such as polysorbate 80 (tween80) can be used to inhibit efflux system, especially P-glycoprotein (P-gp). However, Pgp cannot be completely blocked by low percentage of tween80.

3)-4) Permeabilization of blood brain barrier by toxic effects or surfactants.

5) Opening of the tight junctions. Then, the drug could permeate through the tight junctions in free form or together with the nanoparticles.

6)-7) Nanoparticles can be uptaken by endocytosis by endothelial cells followed by the release of the drugs within these cells and delivery to the brain or by transcytosis through the endothelial cells.

8) A combination of the above effects.

Many studies have reported that nanoparticles can be taken up by receptor-mediated endocytosis, which takes place at the aptical or blood side and transported across the BBB by transcytosis [4, 17, 22]. The particles can then be delivered towards the endothelial cells by intracellular vesicular trafficking and exocytosed at the opposite surface [4]. However, the detailed mechanism of nanoparticles uptake and transcytosis remains unclear [23, 24].

Surface modification of nanoparticles with specific targeted motifs is necessary for facilitating the uptake of nanoparticles [17]. On top of that**, surface properties of nanoparticles**, including properties of coating surfactant, core polymer, drugs and stabilizers, play the most important role for their ability to deliver drugs to the brain [16, 25, 26]. Several studies have investigated the drug transport across BBB by covalent attachment of **targeting motifs** such as apoA1, B, E, insulin, anti-insulin receptor monoclonal antibody (29B4), transferrin, anti-transferrin antibody to nanoparticles [8, 27-30]. Due to the fact that these motifs can specifically interact with specific receptors, for example, apoB and E with LDL receptor, apoA-I with the scavenger receptor class B typeI (SR-BI) [31], the conjugated nanoparticles would mimic lipoprotein particles and enter and across brain endothelial cells by endocytosis and transcytosis[16]. In particular, apolipoprotein (ApoE) has gained more interest in many recent studies. The Apo E protein specifically binds to a number of receptors on the endothelial cell membrane of BBB, such as LDLR, LRP-1, very low density lipoprotein receptor (VLDLR), apolipoprotein receptor-2 (Apo ER-2) and megalin/gp330, as well as receptors in other parts of central nervous system [17]. Thus, the presence of ApoE on the nanoparticle surface can promote the internalization of nanoparticles in the brain endothelial cells via the LDL receptors expressed by these cells [17]. Moreover, ApoE, especially ApoE3 and ApoE4 isoforms, also play the major role of amyloid-β (Aβ) aggregation and clearance which relate to progression of Alzheimer's disease (AD) [32, 33]. So, it is probable that ApoE conjugated nanoparticles can be used to facilitate BBB uptake and target AD disease cells at the same time.

1.5 STATEMENT OF WORK

In this work, apolipoprotein E3 (ApoE3) was employed as a targeting motif in the self-assembly process with two types of polymer, poly (4-vinylpyridine) (P4VP) and poly(caprolactone-grafted-pyridine) (PCL-pyridine) in order to form protein-polymer core shell nanoparticles (ApoE3-NPs). The ApoE3 was also modified with fluorescein dye and self-assembled with the same types of polymer forming fluorescently labelled protein-polymer core shell nanoparticles (Fl-ApoE3-NPs). The uptake of Fl-ApoE3-NPs in a blood brain barrier cell model, human umbilical vein endothelial cells (HUVECs), was studied and is discussed.

REFERENCES

1. Abbott, N.J., Ronnback, L., & Hansson, E. (2006). Astrocyte-endothelial interactions at the blood-brain barrier. *Nature Reviews Neuroscience, 7*(1). 41-53.

2. Nishitsuji, K., Hosono, T., Nakamura, T., Bu, G., & Michikawa, M. (2011). Apolipoprotein E regulates the integrity of tight junctions in an isoform-dependent manner in an in vitro blood-brain barrier model. *The Journal of Biological Chemistry. 286*(20). 17536-17542.

3. Abbott, N.J., Patabendige, A.A., Dolman, D.E., Yusof, S.R., & Begley, D.J. (2010). Structure and function of the blood brain barrier. *Neurobiology of Disease, 37*(1). 13-25.

4. Georgieva, J.V., Hoekstra, D., & Zuhorn, I.S. (2014). Smuggling Drugs into the Brain: An Overview of Ligands Targeting Transcytosis for Drug Delivery across the Blood-Brain Barrier. *Pharmaceutics. 6*(4). 557-583.

5. Deeken, J.F., & Löscher, W. (2007). The blood-brain barrier and cancer: transporters, treatment, and Trojan horses. *Clinical Cancer Research. 13*(6). 1663-1674.

6. Pardridge, W.M. (2005). The Blood-Brain Barrier: Bottleneck in Brain Drug Development. *NeuroRx. 2*(1). 3-14.

7. Löscher, W., & Potschka, H. (2005). Blood-Brain Barrier Active Efflux Transporters: ATP-Binding Cassette Gene Family. *NeuroRx. 2*(1). 86-98.

8. Shilo, M., Motiei, M., Hana, P., & Popovtzer, R. (2014).Transport of nanoparticles through the blood-brain barrier for imaging and therapeutic applications. *Nanoscale. 6*(4). 2146-2152.

9. Denora, N., Trapani, A., Laquintana, V., Lopedota, A., & Trapani, G. (2009). Recent advances in medicinal chemistry and pharmaceutical technology--strategies for drug delivery to the brain. *Current Topics in Medicinal Chemistry. 9*(2). 182-196.

10. Gao, J.Q., Lv, Q., Li, L.M., Tang, X.J., Li, F.Z., Hu, Y.L., & Han, M. (2013). Glioma targeting and blood-brain barrier penetration by dual-targeting doxorubincin liposomes. *Biomaterials. 34*(22). 5628-5639.

11. Roney, C., Kulkarni, P., Arora, V., Antich, P., Bonte, F., Wu, A., Mallikarjuana, N.N., Manohar, S., Liang, H.F., Kulkarni, A.R., Sung, H.W., Sairam, M., & Aminabhavi, T.M. (2005). Targeted nanoparticles for drug delivery through the blood-brain barrier for Alzheimer's disease. *Journal of Controlled Release. 108*(2-3). 193-214.

12. Su, X., Wang, Z., Li, L., Zheng, M., Zheng, C., Gong, P., Zhao, P., Ma, Y., Tao, Q., & Cai, L. (2013). Lipid-polymer nanoparticles encapsulating doxorubicin and 2'-deoxy-5-azacytidine enhance the sensitivity of cancer cells to chemical therapeutics. *Molecular Pharmaceutics. 10*(5). 1901-1909.

13. Singh, R., & Lillard, J.W., Jr. (2009). Nanoparticle-based targeted drug delivery. *Experimental and Molecular Pathology. 86*(3). 215-223.

14. Wilczewska, A.Z., Niemirowicz, K., Markiewicz, K.H., & Car, H. (2012). Nanoparticles as drug delivery systems. *Pharmacological Reports. 64*(5). 1020-1037.

15. Schafer, V., Von, B.H., Rübsamen-Waigmann, H., Steffan, A.M., Royer, C., & Kreuter, J. (1994). Phagocytosis and degradation of human serum albumin microspheres and nanoparticles in human macrophages. *Journal of Microencapsulation : Micro and Nano Carriers. 11*(3). 261-269.

16. Kreuter, J. (2014). Drug delivery to the central nervous system by polymeric nanoparticles: What do we know? *Advanced Drug Delivery Reviews. 71*. 2-14.

17. Wohlfart, S., Gelperina, S., & Kreuter, J. (2012). Transport of drugs across the blood-brain barrier by nanoparticles. *Journal of Controlled Release. 161*(2). 264-273.

18. Yang, H. (2010). Nanoparticle-mediated brain-specific drug delivery, imaging, and diagnosis. *Pharmaceutical Research. 27*(9). 1759-1771.

19. Wohlfart, S., Gelperina, S., & Kreuter, J. (2012). Transport of drugs across the blood brain barrier by nanoparticles. *Journal of Controlled Release. 161*(2). 264-273.

20. Kreuter, J. (2001). Nanoparticulate systems for brain delivery of drugs. *Advanced Drug Delivery Reviews. 47*(1). 65-81.

21. Kreuter, J. (2012) Nanoparticulate systems for brain delivery of drugs. *Advanced Drug Delivery Reviews. 64*. 213-222.

22. Ye, D., Raghnaill, M.N., Bramini, M., Mahon, E., Åberg, C., Salvati, A., & Dawson, K.A. (2013). Nanoparticle accumulation and transcytosis in brain endothelial cell layers. *Nanoscale. 5*(22). 11153-11165.

23. Bramini, M., Ye, D., Hallerbach, A., Raghnaill, M.N., Salvati, A., Aberg, C., & Dawson, K.A. (2014). Imaging approach to mechanistic study of nanoparticle interactions with the blood-brain barrier. *ACS Nano. 8*(5). 4304-4312.

24. Sakhtianchi, R., Minchin, R.F., Lee, K.B., Alkilany, A.M., Serpooshan, V., & Mahmoudi, M. (2013). Exocytosis of nanoparticles from cells: Role in cellular retention and toxicity. *Advances in Colloid and Interface Science. 201–202*. 18-29.

25. Gelperina, S., Maksimenko, O., Khalansky, A., Vanchugova, L., Shipulo, E., Abbasova, K., Berdiev, R., Wohlfart, S., Chepurnova, N., & Kreuter, J. (2010). Drug delivery to the brain using surfactant-coated poly(lactide-co-glycolide) nanoparticles: Influence of the formulation parameters. *European Journal of Pharmaceutics and Biopharmaceutics. 74*(2). 157-163.

26. Wohlfart, S., Khalansky, A.S., Gelperina, S., Maksimenko, O., Bernreuther, C., Glatzel, M., & Kreuter, J. (2011). Efficient chemotherapy of rat glioblastoma using doxorubicin-loaded PLGA nanoparticles with different stabilizers. *PLoS One. 6*(5). ID e19121.

27. Kratzer, I., Wernig, K., Panzenboeck, U., Bernhart, E., Reicher, H., Wronski, R., Windisch, M., Hammer, A., Malle, E., Zimmer, A., & Sattler, W. (2007). Apolipoprotein A-I coating of protamine-oligonucleotide nanoparticles increases particle uptake and transcytosis in an in vitro model of the blood-brain barrier. *Journal of Controlled Release. 117*(3). 301-311.

28. Mulik, R.S., Mönkkönen, J., Juvonen, R.O., Mahadik, K.R., & Paradkar, A.R. (2010). ApoE3 mediated poly(butyl) cyanoacrylate nanoparticles containing curcumin: study of enhanced activity of curcumin against beta amyloid induced cytotoxicity using in vitro cell culture model. *Molecular Pharmaceutics. 7*(3). 815-825.

29. Mulik, R.S., Mönkkönen, J., Juvonen, R.O., Mahadik, K.R., & Paradkar, A.R. (2012). ApoE3 mediated polymeric nanoparticles containing curcumin: apoptosis induced in vitro anticancer activity against neuroblastoma cells. *International Journal of Pharmaceutics. 437*(1-2). 29-41.

30. Ulbrich, K., Knobloch, T., & Kreuter, J. (2011). Targeting the insulin receptor: nanoparticles for drug delivery across the blood-brain barrier (BBB). *Journal of Drug Targeting. 19*(2). 125-132.

31. Wagner, S., Zensi, A., Wien, S.L., Tschickardt, S.E., Maier, W., Vogel, T., Worek, F., Pietrzik, C.U., Kreuter, J., & Von B.H. (2012). Uptake mechanism of ApoE-modified nanoparticles on brain capillary endothelial cells as a blood-brain barrier model. *PLoS One. 7*(3). ID e32568.

32. Frieden, C., & Garai, K. (2012). Structural differences between apoE3 and apoE4 may be useful in developing therapeutic agents for Alzheimer's disease. *Proceedings of the National Academy of Sciences of the United States of America. 109*(23). 8913-8918.

33. Kim, J., Basak, J.M., & Holtzman, D.M. (2009). The role of apolipoprotein E in Alzheimer's disease. *Neuron. 63*(3). 287-303.

CHAPTER 2

PURIFICATION OF APOLIPOPROTEIN E AND SYNTHESIS OF FLUORESCENTLY LABELLED APOE3 (FL-APOE3)

2.1 APOLIPOPROTEIN E

Human apolipoprotein E protein (ApoE) is a polymorphic glycoprotein of 299 amino acids with a molecular weight of 34 kDa [1-4]. It is produced by several cell types but highly expressed in the liver and central nervous system (CNS), especially in astrocytes and microglia [2, 5]. ApoE is a major apolipoprotein in brain and plays an important role in the transportation of lipoprotein, cholesterol and other essential lipids to brain via ApoE receptors which are members of low-density lipoprotein receptor (LDLR) family, including LDLP and LRP1 [1, 5-7]. It also functions as a ligand in receptor mediated endocytosis of lipoprotein particles in the CNS [2, 5].

ApoE proteins have 3 different isoforms which differ by only one or two amino acids: ApoE2 (Cys112, Cys158), ApoE3 (Cys112, Arg158) and ApoE4 (Arg112, Arg158), these differences vary ApoE structure and function (Figure 2.1a, c and Table 2.1) [1, 3-5]. All isoforms are coded from the same ApoE gene but expressed from different alleles (ε2, ε3, ε4): ε2 is associated with a lower risk for Alzheimer's disease (AD) [4, 5], ε3 is the most common isoform found in human [2, 4], and ε4 is a strong risk factor of AD. In addition, the risk of AD increases approximately three fold in people with one ε4 allele and 12-fold in those with two ε4 alleles [4, 5, 7]. There are other forms of apolipoproteins, e.g.

ApoA-I, ApoA-II, ApoA-IV, ApoD, ApoH and ApoJ, which can also be found in the brain [2]. Among them, ApoE is very important to the drug development of neurodegenerative diseases because there are evidences from human and animal studies which indicated that the differences in ApoE isoform differentially affect Aβ aggregation and clearance in the brain, a critical factor for AD therapy [1, 5]. The structure of ApoE (Figure 2.1a, c) shows that there are two major functional domains with the 22-kDa N-terminal domain consisting of four-helix bundle and containing the receptor-binding region on helix 4 (amino acid residues 136-150) and the 10-kDa C-terminal domain consisting of two α-helices and encompassing the lipid-binding region (amino acid residues 244-272) [3, 4, 8]. Two domains are linked by a protease sensitive "hinge region" (amino acid residues 167-206) [3] (Figure 2.1a). Three different isoforms of ApoE are distinguished by two polymorphic positions at amino acid residue 112, 158 [1]. Structural difference of ApoE3 and ApoE4 is a salt bridge between Arg-61 and Glu-255 that plays an important role in maintaining the structure of ApoE4 [4, 8] (Figure 2.1c). More details about differences of ApoE isoforms can be found in Table. 2.1.

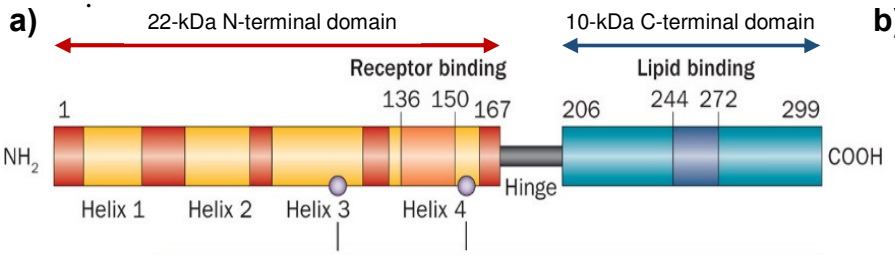

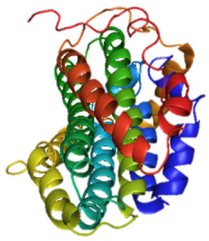

	Isoform-specific amino acid difference		Allele frequency (%)	
	112	158	General	AD
Apo-E2	Cys	Cys	8.4	3.9
Apo-E3	Cys	Arg	77.9	59.4
Apo-E4	Arg	Arg	13.7	36.7

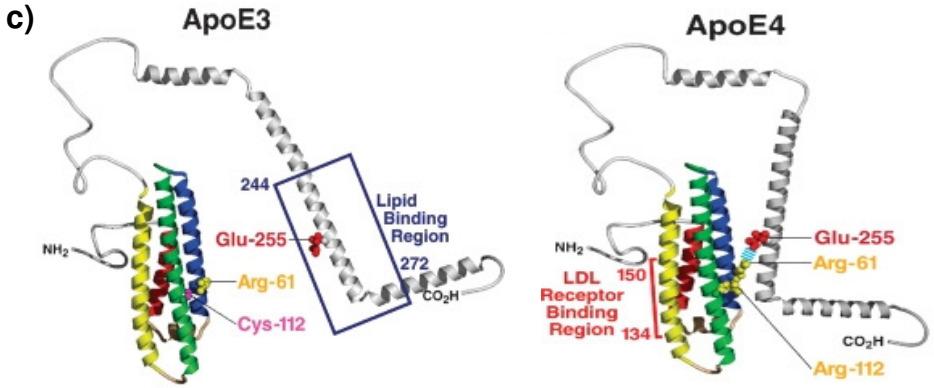

Figure 2.1. a) ApoE3 has two structural domains, N-terminal domain (red) which contains receptor binding region and C-terminal domain (blue) which contains lipid binding region. Those two domains are linked by hinge region (gray). ApoE2, E3 and E4 isoforms are encoded by the ε2, ε3 and ε4 alleles on ApoE gene respectively. There are two polymorphic positions, 112 and 158, that distinguish the three common isoforms. Figure is adapted with permission from Liu, C-C. *et al* (2013) *Nat Rev Neurol*, 9, 106-118. **b)** The model structure illustrating the full length human ApoE3 created by Chen, J. *et al* (2011) *Proc. Natl. Acad. Sci,* 108, p.14813. Solution NMR method was used in studying the structure of the ApoE3 and the picture was produced by PyMOL. **c)** Model of the structure of ApoE3 and ApoE4 and structural difference of ApoE3 and ApoE4. Key structural elements of ApoE are N-terminal domain which contains a four helix bundle (helix1, red; helix2, blue; helix3, green; helix4, yellow) and C-terminal domain (gray) which contains lipid binding elements. Main differences is a putative salt bridge between Arg-61 and Glu-255 presenting only in ApoE4 that stabilizes a closer contact between the N- and C- terminal domains. Figure is adapted with permission from Hatter, D.M. *et al* (2006) *Trends Biochem Sci*, 31, 445-454.

Table 2.1 Prevalence of the human ApoE isoforms and their key differences. Adapted with permission from Hatter, D.M. *et al* (2006) *Trends Biochem Sci*, 31, 445-454.

Isoform	Average allelic frequency (%)	Amino acid variation (residue)		Functional differences		Structural differences		Associated disorders
		112	158	LDL receptor affinity	Lipoprotein-binding preference	Conformational stability and folding behavior	Domain interaction?	
ApoE2	7	Cys	Cys	Low	HDL	Most stable and lacks folding intermediates	No	Type III hyperlipoproteinemia
ApoE3	78	Cys	Arg	High	HDL	Intermediate stability with folding intermediates	No	Unknown
ApoE4	15	Arg	Arg	High	VLDL LDL	Least stable with folding intermediates	Yes	Alzheimer's disease and other neurological conditions; atherosclerosis

According to the ability of ApoE to specifically bind LDLR receptor on BBB endothelial cell membrane and the ability of ApoE to internalize within the cells by receptor mediated endocytosis, we believe that ApoE is a good candidate in developing drug carrier targeting BBB. Therefore, in this work, ApoE3, which is the most abundant isoform in human body and ApoE4 which is a risk factor of AD were chosen as targeting motif in the development of protein polymer core-shell nanoparticles (PPCS-NPs). We propose that the capability of ApoE3 in targeting LDLR receptor together with self-assembly protocol which was developed in our lab will generate well-defined PPCS-NPs that can be used to specifically target BBB endothelial cell and further developed as drug delivery vehicles across the BBB in the future. The development of PPCS-NPs will be further explained in next chapter.

2.2 PURIFICATION AND ANALYSIS OF APOLIPOPROTEIN E3 AND E4

Human ApoE3 protein can be obtained from pre-engineered Human embryonic kidney endothelial cell line (HEK 293T cells) which was provided from Dr. Dapin Fan, School of Medicine, University of South Carolina. Briefly, the ApoE coding sequence (954 bp) was sub-cloned into the PWPI-GFP vector using single enzyme (PmeI) insertion and direction screening generating lentiviral ApoE constructs. The lentiviral expression plasmid for human ApoE3 were then transfected into HEK 293T cells using ProFection mammalian transfection system to generate HEK 293T cells that can produce human ApoE3 protein (HEK 293T-ApoE3). The HEK 293T-ApoE3 cells were cultured in DMEM complete growth medium with standard conditions, 5% CO_2 at 37 ^oC. ApoE3 protein was then purified from HEK 293T-ApoE3 culture media by FPLC using heparin-sepharose

CL-6B column and freeze-dried by lyophilization for long-term storage. Typical yield of the purified ApoE3 was about 5 mg/150 mLculture medium. The ApoE3 was further analyzed by SDS-PAGE using gradient (4-20%) gel and stained with Coomassie blue, then confirmed by western blot and MALDI-MS. The molecular weight of ApoE3 is slightly higher than 34 kDa as showed from SDS-PAGE analysis (Figure 2.2a). Two faint bands below 34 kDa can also be seen on the gel. We assumed that they were degraded partial fragments of ApoE3 after purification process, probably, N-terminal and C-terminal based on approximate molecular weight. This assumption correlated to special structure of ApoE3 protein which contained two terminal domains linked to each other by protease sensitive hinge region [3, 9]. The purity of the purified ApoE3 was estimated to be ~85% based on the result from SDS-PAGE analysis. The identity of human ApoE3 was confirmed by Western blot analysis of purified ApoE3 against primary antibody, Goat anti human ApoE, and secondary antibody, Fab anti-goat IgG (Donkey antibody). The result showed ApoE expression in purified ApoE3 solution at the molecular weight of about 34, 22 and 10 kDa (Figure 2.2b). Molecular weight of ApoE3 was further confirmed by MALDI-MS anlysis. The molecular weight of unmodified full-length ApoE3 was 35,085.56 m/z (Figure 2.2c, red arrow) comparing to the theoretical molecular weight of human ApoE protein which was 34,236 Da (Uniprot). However, the molecular weight of ApoE3 from MS analysis may not be very accurate due to broad peaks and low signal intensity. The MALDI-MS result correlated to the SDS-PAGE analysis, however the difference in molecular weight of the purified ApoE3 may probably came from genetic modification process producing HEK 293T-ApoE3 cells. For peptide analysis, ApoE3 was incubated with trypsin at 37 ^{o}C for 4 h, then analysed by MALDI-MS. The peptide analysis

peak list (Figure 2.2d) was generated by FlexAnalysis software and interpreted by MASCOT software. The result showed that the purified ApoE3 soluiton was identical to the full length ApoE3 with a 62% of protein sequence coverage (Figure 2.2e) and the MASCOT score of 75 confirming the identity of the purified protein as ApoE3.

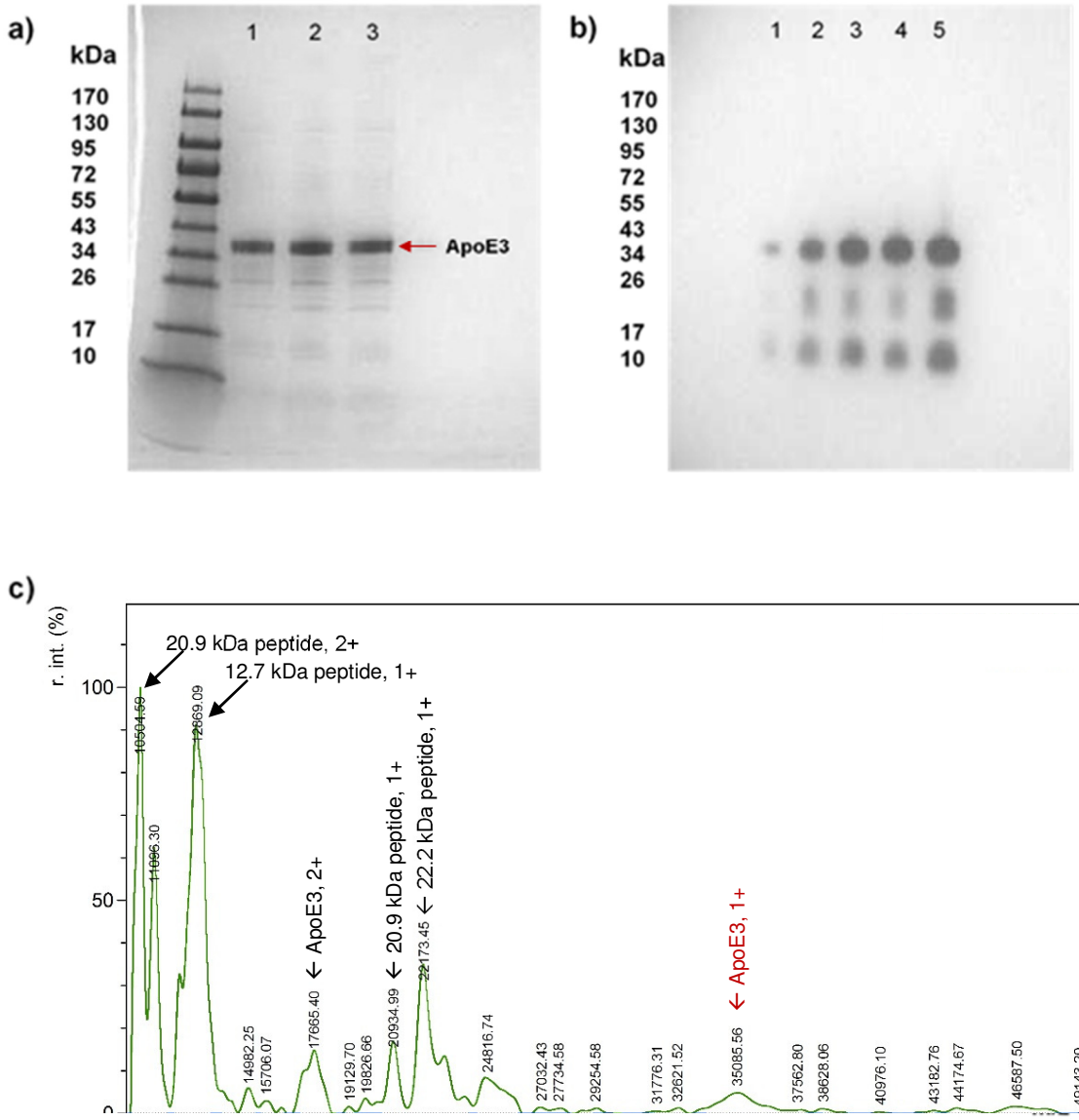

d)

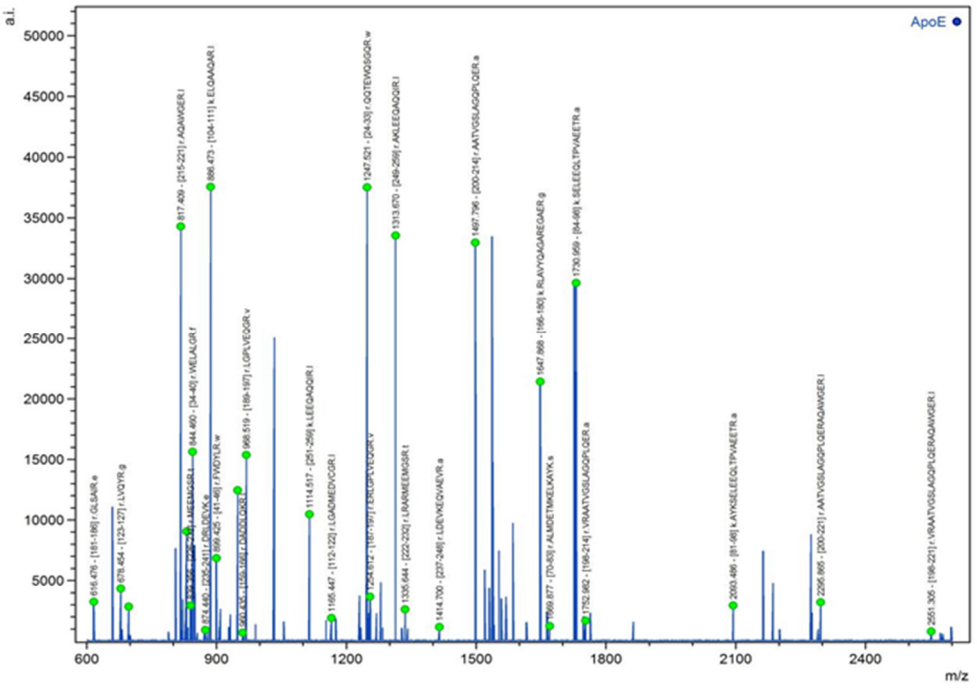

e)

```
  1 HHHHHHHHKV EQAVETEPEP ELRQQTEWQS GQRWELALGR FWDYLRWVQT
 51 LSEQVQEELL SSQVTQELRA LMDETMKELK AYKSELEEQL TPVAEETRAR
101 LSKELQAAQA RLGADMEDVC GRLVQYRGEV QAMLGQSTEE LRVRLASHLR
151 KLRKRLLRDA DDLQKRLAVY QAGAREGAER GLSAIRERLG PLVEQGRVRA
201 ATVGSLAGQP LQERAQAWGE RLRARMEEMG SRTRDRLDEV KEQVAEVRAK
251 LEEQAQQIRL QAEAAQARLK SRFEPLAEDM QRQWAGQVEK VQAAEGTSAA
301 PVPSDNH
```

Figure 2.2. a) SDS-PAGE analysis of the purified ApoE3. Protein were analyzed on a gradient (4-20%) gel and stained with Coomassie blue. Lane 1, ApoE3 with a concentration of 2.52 µg/mL; lane 2, ApoE3 with a concentration of 4.00 µg/mL; Lane 3, ApoE3 with a concentration of 6.00 µg/mL. The molecular weight of ApoE3 was a little higher than 34.0 kDa (Red arrow). **b)** Western blot analysis of purified ApoE3 against 1^{o} antibody, Goat anti human ApoE, and 2^{o} antibody, Fab anti-goat IgG (Donkey antibody), shown ApoE expression at molecular weight of about 34 kDa. Lane 1-5 was ApoE3 with a concentration of 2.0, 4.0, 6.0, 8.0, 10.0 ng/mL. **c)** MALDI-MS analysis of purified ApoE3 showed the molecular mass of unmodified ApoE3 as 35,085.56 m/z (red arrow). **d)** Peptide analysis peak list of ApoE3 created by FlexAnalysis software. **e)** Peptide analysis by MASCOT software, identical residues were highlighted in red with 62% recovery and MASCOT score of 75.

ApoE4 was purified from HEK293T-ApoE4 culture media followed the same procedure as ApoE3. However, the purification of ApoE4 was not successful. The purified eluent still had a lot of impurities as shown by the SDS-PAGE analysis. The impurities may came from contamination during purification process by FPLC including binding condition of protein to column, running and elution buffer condition or protein degradation during purification process and storage technique. Another possible reason is problem with protein expression in HEK293T-ApoE4 cells. MALDI-MS analysis was also inconclusive.

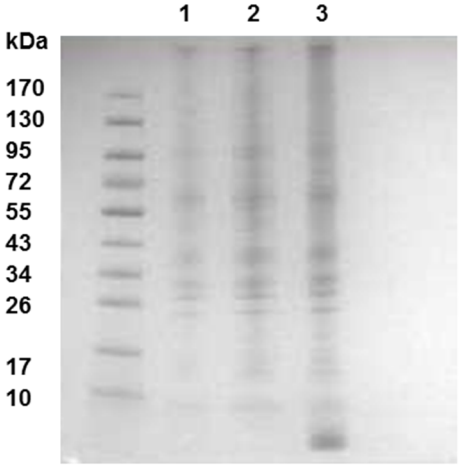

Figure 2.3. ApoE4 determination by SDS-PAGE. Protein were analyzed on a gradient (4-20%) gel and stained with Coomassie blue. Lane 1, ApoE4 with a concentration of 2.5 µg/mL; Lane 2, ApoE4 with a concentration of 5.0 µg/mL; Lane 3, ApoE4 with a concentration of 9.90 µg/mL. The result showed a lot of impurities indicated that the purification process was not successfully done.

2.3 SYNTHESIS OF FLUORESCENTLY LABELED APOE3

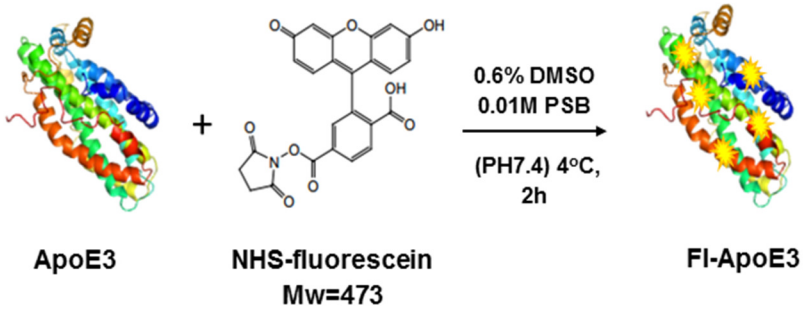

Figure 2.4. Schematic illustration of the synthesis of Fl-ApoE3.

NHS-fluorescein conjugated ApoE3 (Fl-ApoE3) was synthesized and its molecular weight was analyzed by SDS-PAGE using a gradient (4-20%) gel and staining with Coomassie blue. The gel was visualized under the EPI white light comparing to under the UV-VIS light in order to detect the fluorescent signal on the protein bands. Fluorescent signal can be detected under UV-VIS only in Fl-ApoE3 not in unmodified ApoE3. The result showed that molecular weight of Fl-ApoE3 was a little higher than 34 kDa (Figure 2.5). Fl-ApoE3 was further analyzed by MALDI-MS, the molecular weight of Fl-ApoE3 was 35,128.53 m/z (Figure 2.6, red arrow). The result showed that there were about 2 fluorescein molecules conjugated on an ApoE3 protein, comparing to the theoretical molecular weight of ApoE3. If the fluorescein molecules were successfully conjugated to ApoE3 at all 13 lysine residues, the theoretical molecular weight of Fl-ApoE3 would increase to 40,390 Da. The broad peak as showed in the result and low signal intensity was assumed to cause inaccurate molecular weight. The resultant proteins were used in the co-assembly study with selected polymers as described in the consequent chapter.

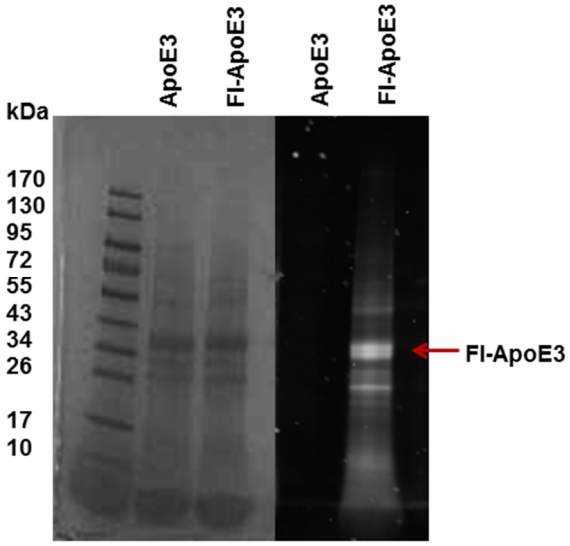

Figure 2.5. Fl-ApoE3 identification by SDS-PAGE visualized under EPI white (left) and UV-VIS (right). Fluorescent signal can only be seen in the lane loaded with Fl-ApoE3. The molecular mass of Fl-ApoE3 was approximately about 34 kDa.

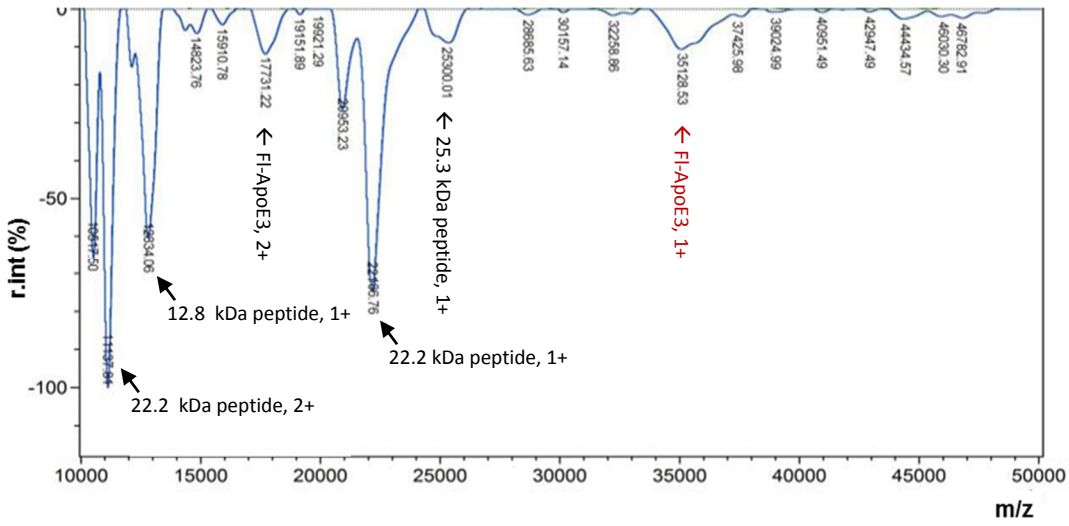

Figure 2.6. MALDI-MS analysis of Fl-ApoE3 showed the molecular mass of Fl-ApoE3 was 35,128.53 m/z (red arrow).

2.4 CONCLUSION

ApoE3 can be purified from HEK 293T-ApoE3 culture media by FPLC and freeze-dried for long-term usage. ApoE3 was successfully produced in a large quantity (~5.0 mg/150 mL culture media) and high purity. The molecular weight of purified ApoE3 which was identified by SDS-PAGE was approximately 34 kDa. The identity of purified ApoE3 was further confirmed by western blot analysis, MALDI-MS, and peptide analysis. The molecular mass of ApoE3 form MALDI-MS was 35,085.56 m/z which was consistant to the theoretical mass. We did not successfully purified ApoE4, even though we have tried to optimize the conditions of the purification process. Fl-ApoE3 was successfully synthesized and analyzed by SDS-PAGE and MALDI-MS. The result from SDS-PAGE showed molecular mass of Fl-ApoE3 was a little bit higher than 34 kDa and the result from MALDI-MS showed the molecular mass of Fl-ApoE3 was 35,128.53 m/z. Both ApoE3 and Fl-ApoE3 would be further used in self-assembly process with selected polymers to form protein-polymer core-shell nanoparticles for the BBB cellular uptake study.

2.5 MATERIALS AND METHOD

MATERIALS

HEK 293T-ApoE3 and HEK 293T-ApoE4 cell line were obtained from Dr.Daping Fan (University of South Carolina, School of Medicine), Dulbecco's modified Eagle's medium (DMEM) and fetal bovine serum (FBS) was purchased from VWR. Trypsin/ EDTA solution and penicillin-streptomycin (P/S) was purchased from Hyclone. Mini-Protein TGX Stain-free Procast Gel (4-20%), 10 well-comb, 50 µL/well was purchased from Bio-Rad. Tris-Glycine-SDS, 10X Solution (Electrophoresis) was purchased from Fisher Scientific. LabSafe gel blue was purchased from VWR. EZ-Run™ Prestained Rec Protein Ladder was purchased from Fisher Scientific. Trypsin from bovine pancreas was purchased from Sigma-Aldrich. NHS-fluorescein was purchased from Pierce. Snake skin dialysis tubing 3.5K was purchased from Fisher Scientific. Nanosep 10K was purchased from Pall. All the reagents were used as receive.

APOE3 HARVESTING

The HEK293T-ApoE3 cell line, which can produce Apolipoprotein E3, was obtained from Dr.Daping Fan (University of South Carolina, School of Medicine). The 293T-ApoE3 Cells were maintained in two of 75 mm^2 flasks in DMEM-high glucose medium with 10% FBS and 1% P/S in a water-saturated atmosphere of 5% CO_2 and 95% air at 37 °C until it reaches 80% confluent. Then, the cells were split into twenty 100 mm^2 dishes and cultured in complete growth medium with 10% FBS for two days. The cells would be about 80% confluent, then changed the media to 1% FBS/DMEM/high glucose and incubated for 24 h. The cell culture media were harvested in 250 mL Nalgene

centrifuge bottles, centrifuged at 5,000 rpm for 10 min in the SLA-1500 rotor. The media were aliquoted to labeled 50 mL tubes and kept at -80 °C or use immediately for purification by FPLC.

APOE4 HARVESTING

The HEK293T-ApoE4 cell line, which can produce Apolipoprotein E4, was obtained from Dr. Daping Fan (University of South Carolina, School of Medicine). The 293T-ApoE4 Cells were maintained in the same condition and follow the ApoE3 harvesting protocol.

APOE3 PURIFICATION

ApoE3 can be purified from the media that were collected from HEK293T-ApoE3 cells by using a Heparin-Sepharose CL-6B column for purification, 200 mM NaCl in 10mM sodium phosphate buffer pH 7.4 as running buffer and 1M NaCl in 10mM sodium phosphate buffer pH 7.4 as elution buffer. Then, the selected fractions were pooled and dialyzed against 4 liters of 10 mM ammonium bicarbonate at 4 °C over night with two buffer changes. The purified ApoE3 could be freeze-dried by lyophilization and kept in -20 °C for further use.

APOE4 PURIFICATION

ApoE4 can be purified from the media that were collected from HEK293T-ApoE3 cells by using a Heparin-Sepharose CL-6B column for purification, 200, 300, 400, 600, 800 mM NaCl in 10mM sodium phosphate buffer pH 7.4 as running buffer and 1M NaCl in 10mM sodium phosphate buffer pH 7.4 as elution buffer.

APOE3 ANALYSIS

The molecular weight of ApoE3 was determined by SDS-PAGE, using a gradient (4-20%) gel, running at 200 V for 30 min and stained with Coomassie blue. The result can be confirmed by MALDI-MS analysis which was done by Dr.Yuzhe Nie. For MS analysis, ApoE3 protein solution in water was mixed in a ratio of 1:1 with 20 mg/mL α-cyano-4-hydroxycinnamic acid matrix (CHCA matrix) in 70% acetonitrile (CAN) containing 0.1% trifluoroacetic acid (TFA). The mixture was spotted on the MTP AnchorChip target TM 600/384TF (Bruker Daltonics), spectra were then acquired in the m/z range of 10,000-50,000 with Ultraflex TOF/TOF (Bruker Daltonics) MALDI time-of-flight mass spectrometer. The spectrometer was operated in a linear positive ion mode with a laser frequency of 20 Hz and 100% relative energy. External calibration was done based on the average value of [M+H+] of BSA, m/z of 66,463. A total of 20,000 shots were used to generate a spectrum from the spots. The export mass data was analyzed by mMass software. Moving average smooth method was used to get better S/N with widow size 250 m/z. ApoE3 peptide analysis was done with help from Dr. Xiaolei Zhang. Brieftly, ApoE3 was extracted from SDS gel and incubated with trypsin at 37 ^{o}C for 4 h and further analyzed by MALDI-MS. ApoE3 was also identified by western blot analysis against primary

antibody, Goat anti human ApoE, and secondary antibody, Fab anti-goat IgG (Donkey antibody).

FLUORESCENT-CONJUGATED PROTEINS

A solution of NHS-fluorescein in DMSO (50 μL; 1 mg mL^{-1}) was slowly added (1 drop/10 s) into a solution of protein (2 mg mL^{-1} in PBS buffer pH 7.4) at 4 ^{o}C with gently stirring. The solution mixture was incubated in dark at 4 ^{o}C for 2 h. Then, the excess NHS-fluorescein was removed by using nanosep centrifugal system with Mw cutoff 10 kDa, centrifuged at 5,000 × g for 5 mins, 2 times. The fluorescein conjugated protein was analyzed by SDS-PAGE.

REFERENCES

1. Liu, C-C., Kanekiyo, T., Xu, H., & Bu, G. (2013). Apolipoprotein E and Alzheimer disease: risk, mechanisms and therapy. *Nature Reviews Neurology. 9*(2). 106-118.

2. Kim, J., Basak, J.M., & Holtzman, D.M. (2009). The role of apolipoprotein E in Alzheimer's disease. *Neuron. 63*(3). 287-303.

3. Frieden, C., & Garai, K. (2012). Structural differences between apoE3 and apoE4 may be useful in developing therapeutic agents for Alzheimer's disease. *Proceedings of the National Academy of Sciences of the United States of America.109*(23). 8913-8918.

4. Chou, C.Y., Lin, Y.L., Huang, Y.C., Sheu, S.Y., Lin, T.H., Tsay, H.J., Chang, G.G., & Shiao M.S. (2005). Structural Variation in Human Apolipoprotein E3 and E4: Secondary Structure, Tertiary Structure, and Size Distribution. *Biophysical Journal. 88*(1). 455-466.

5. Holtzman, D.M., Herz, J., & Bu, G. (2012). Apolipoprotein E and apolipoprotein E receptors: normal biology and roles in Alzheimer disease. *Cold Spring Harb Perspect Med. 2*(3): ID a006312.

6. Michaelis, K., Hoffmann, M.M., Dreis, S., Herbert, E., Alyautdin, R.N., Michaelis, M., Kreuter, J., & Langer, K. (2006). Covalent linkage of apolipoprotein e to albumin nanoparticles strongly enhances drug transport into the brain. *Journal of Pharmacology and Experimental Therapeutics. 317*(3). 1246-1253.

7. Nishitsuji, K., Hosono, T., Nakamura, T., Bu, G., & Michikawa, M. (2011). Apolipoprotein E regulates the integrity of tight junctions in an isoform-dependent manner in an in vitro blood-brain barrier model. *The Journal of Biological Chemistry. 286*(20). 17536-17542.

8. Hatters, D.M., Peters-Libeu, C.A., & Weisgraber, K.H. (2006). Apolipoprotein E structure: insights into function. *Trends in Biochemical Sciences. 31*(8). 445-454.

9. Wetterau, J.R., Aggerbeck, L.P., Rall, S.C., Jr., & Weisgraber, K.H. (1988). Human apolipoprotein E3 in aqueous solution. I. Evidence for two structural domains. The Journal of Biological Chemistry. 263(13). 6240-6248.

CHAPTER 3

SELF-ASSEMBLY AND CELL UPTAKE OF PROTEIN POLYMER CORE SHELL NANOPARTICLES

3.1 INTRODUCTION

It is very challenging to develop drug delivery carriers to deliver payloads to brain due to the restriction of the blood brain barrier (BBB) [1-3]. To overcome this problem, many researchers are currently focusing on the development of safe and efficient methods that promote the drug delivery across the BBB [3, 4]. One idea is to specifically target the BBB endothelial cells and effectively transport the delivery vehicles across the BBB and subsequently release drug at appropriate sites within the brain [3, 5].

Nanoparticles can help transporting drugs that normally cannot cross BBB [1, 6]. The first developed particles that were reported crossing BBB and led to important pharmacological and therapeutic effects in the brain were the poly(butyl cyanoacrylate) (PBCA) particles coated by polysorbate 80 (Tween80) [1, 2, 7-9]. The nanoparticles could deliver drugs, such as loperamide, tubocurarine, doxorubicin, and peptides, such as hexapeptide, endorphin, dalargin and dipeptide kyotorphin [1, 7, 10]. It was hypothesized that the general toxic effect of polysorbate 80 might disrupt the tight junctions and result in the translocation of nanoparticles across the BBB [3, 11]. However, Kreuter J *et al.* later assumed that the surfactant coated nanoparticles led to the adsorption of apolipoprotein E on the particles' surface thereby mimicking natural lipoproteins and promoting the

interaction with the lipoprotein receptors (LDLR) on the endothelial cells of the BBB [1, 3, 12-14]. The particles would then subsequently endocytose into the cells and transcytose across the BBB [1, 15]. Although the Tween80-PBCA nanoparticles were proved to increase the CNS bioavailability of rivastigmine and tacrine for treating AD, they also showed several disadvantages, including limited drug loading capacity, low rate in *in vivo* biodegradation, and the release of toxic formaldehyde residues [3, 16, 17].

Recently, Michaelis *et al.* developed ApoE coupled with human serum albumin nanoparticles (ApoE-HSA-NPs) for transporting loperamide across the BBB [1]. These biodegradable, surfactant-free nanoparticles can be prepared in defined size and carry reactive groups, such as thiol, amino, and carboxylic groups, on their surfaces that can be used for ligand binding and surface modifications [1]. The ApoE-HAS-NPs were able to transport loperamide across the BBB while the unmodified HAS-NPs cannot do so [1]. This may lead to the conclusion that ApoE conjugated nanoparticles can facilitate drug transport to the brain [1]. A similar study was confirmed by Zensi *et al.*, where the ApoE-HAS-NPs, size of approx. 250 nm, were shown to be uptaken by endothelial cells (*in vivo*) within 15-30 min while pegylated nanoparticles, as a control, did not associate with the cells [3, 18]. Intracellular trafficking was also studied *in vitro* in bEND3 cells, a BBB cell model, and found that ApoE3-HAS-NPs were located in the intracellular compartment after incubation for 2 h [3]. Other apolipoproteins, ApoA-I and ApoB-100 were also used as targeting motifs for loperamide-HAS-NPs. The transportation of these nanoparticles comparing to ApoE-HAS-NPs was studied *in vivo* scored by antinociceptive response 15 min after injection. The result showed that ApoE-HAS-NPs produced the highest transportation effect [3, 19, 20].

Our research group developed a one-step self-assembly protocol to prepare protein-polymer core-shell nanoparticles (PPCS-NPs) with controlled structure and preserved protein activity and conformation [21]. This self-assembly method is based on synergistic interactions between proteins and water insoluble polymers tailored with pyridine units, such as poly(4-vinylpyridine) (P4VP) and pyridine grafted poly(hydroxyethyl methacrylate) (pHEMA) [21]. The process is driven by displacing protein between the interface of water and polymers to minimize the interfacial energy, the same idea as Pickering emulsions [21-23]. Proteins on the surface take part in stabilizing the water-polymer interface, and the hydrogen bonding helps the stabilization of the final structures [21, 22, 24, 25]. We recently developed a new pyridine-grafted polymer, i.e. poly (caprolactone-grafted-pyridine) (PCL-py). Since ApoE3 can facilitate drug delivery across BBB, here we use ApoE3 as a targeting motif, P4VP and PCL-py as polymer components, to fabricate ApoE3 based PPCS-NPs and study the cellular uptake of the nanoparticles in human umbilical vein endothelial cells (HUVECs), a BBB cell model (Figure 3.1).

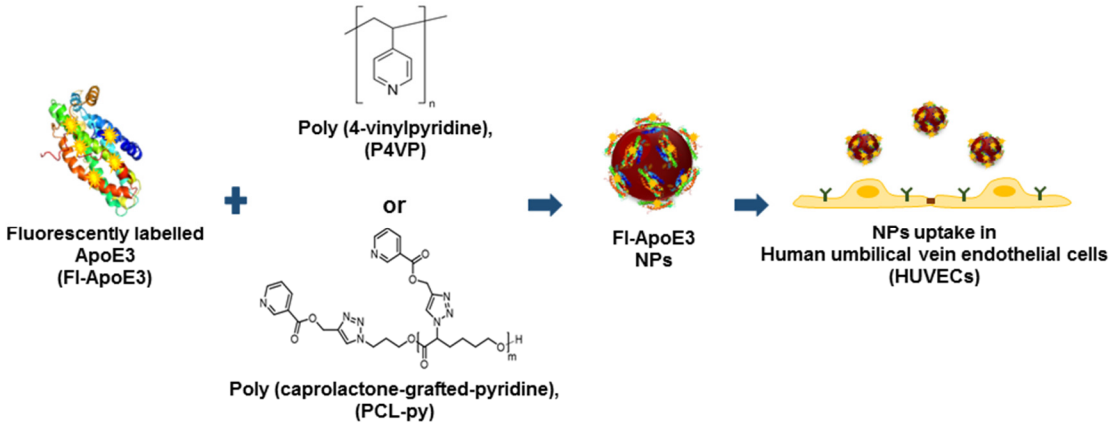

Figure 3.1 Schematic illustration of the formation of Fl-ApoE3 nanoparticles (Fl-ApoE3 NPs) and the study of nanoparticles uptake in HUVECs cells.

3.2 Self-assembly of ApoE3-P4VP Nanoparticles (ApoE3-P4VP-NPs)

Preparation of ApoE3-P4VP-NPs was easily conducted by slowly dropwise the solution of P4VP in ethanol to an aqueous solution of ApoE3 proteins with stirring (Figure 3.2a). The size of the particles were controlled by varying mass ratio between protein and polymer (M_{ApoE3}/M_{P4VP}). We chose three M_{ApoE3}/M_{P4VP}, i.e. 0.60, 1.20 and 2.40, in this study. The size of the particles with different mass ratios was measured by dynamic light scattering (DLS) technique (Figure 3.2b). The average size of ApoE3-P4VP-NPs was ranging from 150-180 nm, polydispersity index (PDI) and zeta potential of the particles are listed in Table. 3.1. TEM imaging was used to confirm the size and spontaneous assembly of proteins and polymers into the PPCS-NPs. As shown in Figure 3.2c-e, the size of the particles measured from TEM corresponded with results from DLS. The TEM result also revealed that the particles seemed to have spherical shapes with well-defined particle morphologies. The CD spectra did not clearly show two minima at 208 and 222 nm [26] (Figure 3.2f), therefore it was unable to reveal the helical structure of ApoE3 or conformational change of the ApoE3 after self-assembly process. One possible reason that CD analysis is inconclusive is an inaccurate concentration of samples that was prepared by serial dilution. Another possible reason is contamination of salt from PBS buffer that was used in self-assembly process.

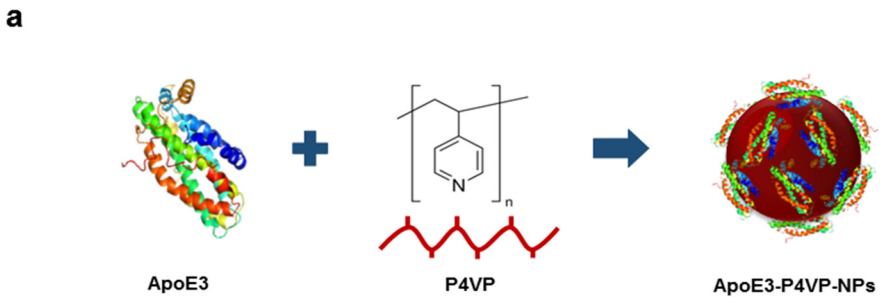

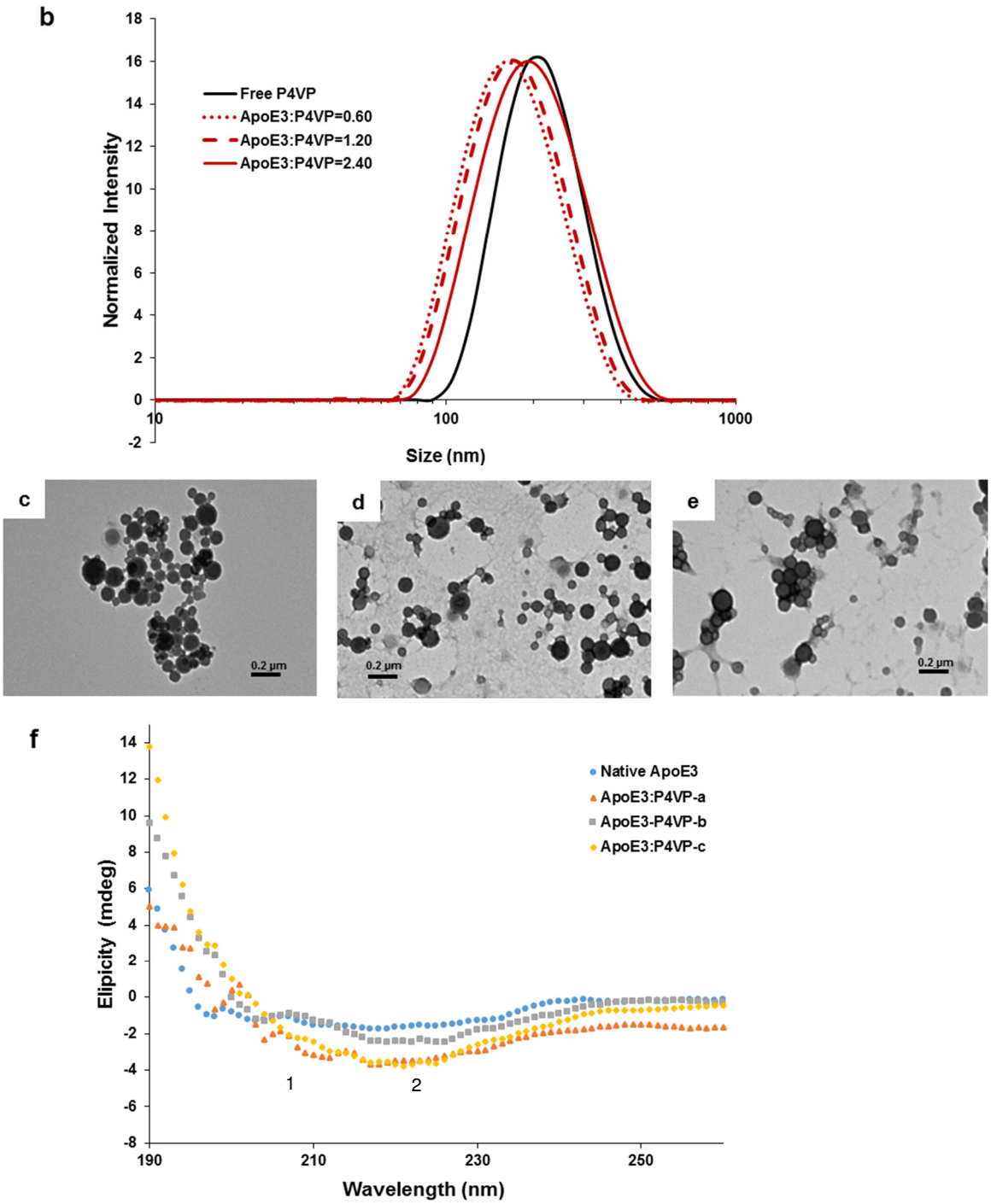

Figure 3.2. **(a)** Schematic illustration of the synthesis of ApoE3-P4VP-NPs. **(b)** DLS results of ApoE3-P4VP-NPs with different mass ratio (M_{ApoE3}/M_{P4VP}): 0.60, 1.20 and 2.40. TEM images of ApoE3-P4VP-NPs at different mass ratio, where **(c)** M_{ApoE3}/M_{P4VP} = 0.60, **(d)** M_{ApoE3}/M_{P4VP} = 1.20, and **(e)** M_{ApoE3}/M_{P4VP} = 2.40. **(f)** Circular dichroism of ApoE3 and ApoE3-P4VP-NPs. ApoE3:P4VP-a: M_{ApoE3}/M_{P4VP} = 0.60; ApoE3:P4VP-b: M_{ApoE3}/M_{P4VP} = 1.20; and ApoE3:P4VP-c: M_{ApoE3}/M_{P4VP} = 2.40. Both native ApoE3 and ApoE3-P4VP-NPs does not clearly show two minima at 208 (1) and 222 (2) nm.

Table 3.1 Sizes of ApoE3-P4VP-NPs measured by DLS (a-c) with different mass ratios of proteins to P4VP (M_{ApoE3}/M_{P4VP}).

System	M_{ApoE3}/M_{P4VP}	Size (nm)	PDI	Zeta potential
Free P4VP	-	204 ± 24	0.091	-9.34
ApoE3-P4VP-a	0.60	148 ± 14	0.116	-19.88
ApoE3-P4VP-b	1.20	166 ± 3	0.150	-20.87
ApoE3-P4VP-c	2.40	184 ± 5	0.133	-20.17

3.3 Self-assembly of Fluorescently labeled ApoE3-P4VP Nanoparticles (Fl-ApoE3-P4VP-NPs)

Preparation of Fl-ApoE3-P4VP-NPs was followed the same method as the preparation of the ApoE3-P4VP-NPs (Figure 3.3a). The size of the particles with mass ratios of $M_{Fl\text{-}ApoE3}/M_{P4VP}$: 0.60, 1.20 and 2.40, were measured by dynamic light scattering (DLS) (Figure 3.3b). The average size was ranging from 135-165 nm as shown in Table. 3.2. TEM imaging results confirmed that the size of the particles was corresponded to the DLS result. They also showed well-defined spherical structure that represented spontaneous assembly of proteins and polymers into the PPCS-NPs as can be seen in Figure 3.3c-e.

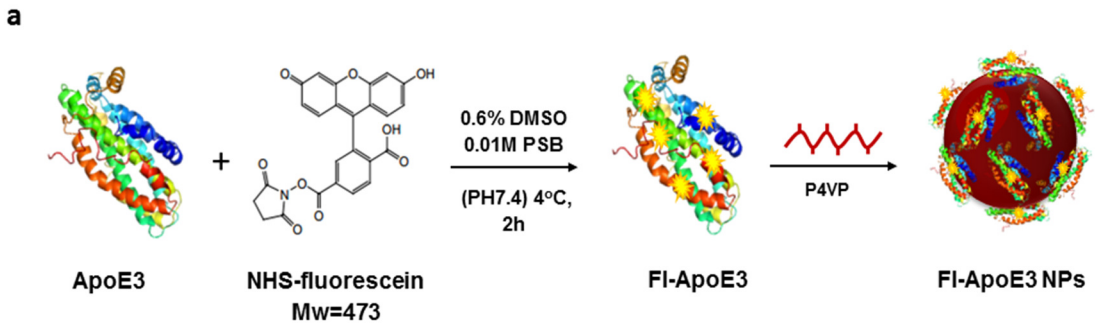

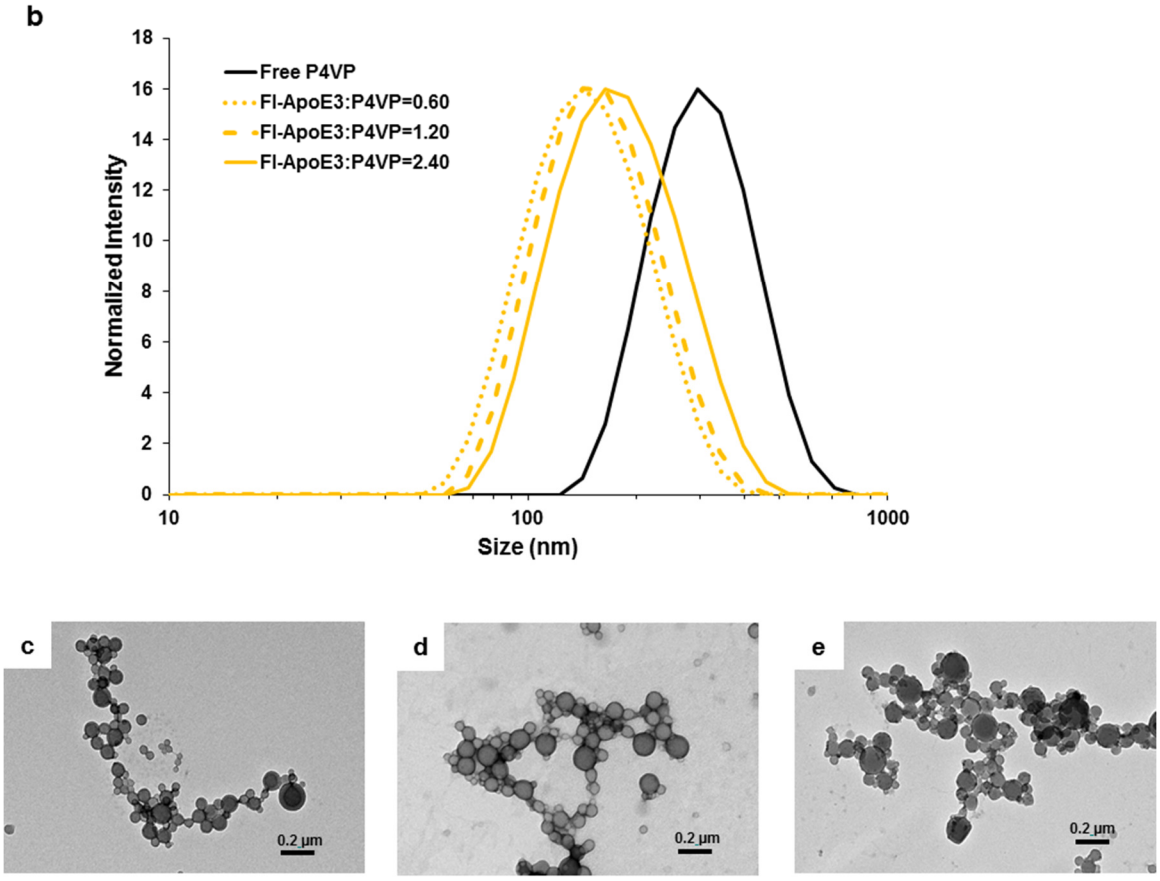

Figure 3.3. **(a)** Schematic illustration of the synthesis of Fl-ApoE3-P4VP-NPs. **(b)** DLS results of Fl-ApoE3-P4VP-NPs with different mass ratio ($M_{Fl\text{-}ApoE3}/M_{P4VP}$: 0.60, 1.20 and 2.40). TEM images of Fl-ApoE3-P4VP-NPs at different mass ratio, where **(c)** $M_{Fl\text{-}ApoE3}/M_{P4VP}$ = 0.60 **(d)** $M_{Fl\text{-}ApoE3}/M_{P4VP}$ = 1.20 **(e)** $M_{Fl\text{-}ApoE3}/M_{P4VP}$ = 2.40.

Table 3.2 Sizes of Fl-ApoE3-P4VP-NPs measured by DLS (a-c) with different mass ratios of proteins to P4VP ($M_{Fl\text{-}ApoE3}/M_{P4VP}$).

System	$M_{Fl\text{-}ApoE3}/M_{P4VP}$	Size (nm)	PDI	Zeta potential
Free P4VP	-	316 ± 28	0.211	-11.38
Fl-ApoE3-P4VP-a	0.60	135 ± 7	0.111	-17.80
Fl-ApoE3-P4VP-b	1.20	147 ± 9	0.114	-20.62
Fl-ApoE3-P4VP-c	2.40	164 ± 5	0.131	-20.07

3.4 SELF-ASSEMBLY OF APOE3-P4VP NANOPARTICLES (APOE3-PCL-PY-NPS)

Preparation of ApoE3-PCL-py-NPs was performed by self-assembly method, the same manner as the preparation of the ApoE3-P4VP-NPs (Figure 3.4a). Three mass ratios of $M_{ApoE3}/M_{PCL\text{-}py}$; 0.60, 1.20 and 2.40 were chosen in this study. The size of synthesized particles were measured by dynamic light scattering (DLS) technique (Figure 3.4b). The average size was ranging from 108-150 nm, polydispersity index (PDI) and zeta potential of the particles were shown in Table. 3.3. TEM imaging was used to confirm the size and spontaneous assembly of proteins and polymers into the PPCS-NPs. TEM images illustrated the ApoE3-PCl-py-NPs in spherical shape with small size distribution (Figure 3.4c-e). The conformational change of the ApoE3 protein on the surface of the particles was studied by circular dichroism (CD). However, CD spectra as shown in Figure 3.2f was not good enough to tell conformational change of ApoE3. We still believe that it is because an inaccurate concentration of samples that was prepared by serial dilution and contamination of salt from PBS buffer that was used in self-assembly process. Also, degradation of protein or nanoparticles may be another possible reason.

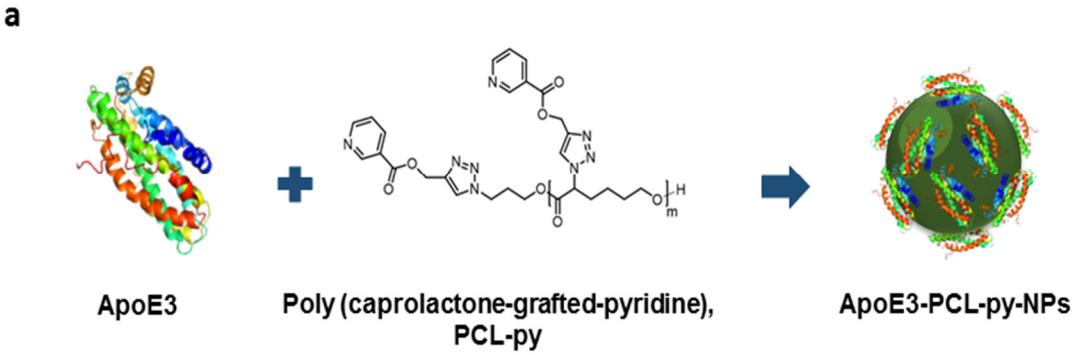

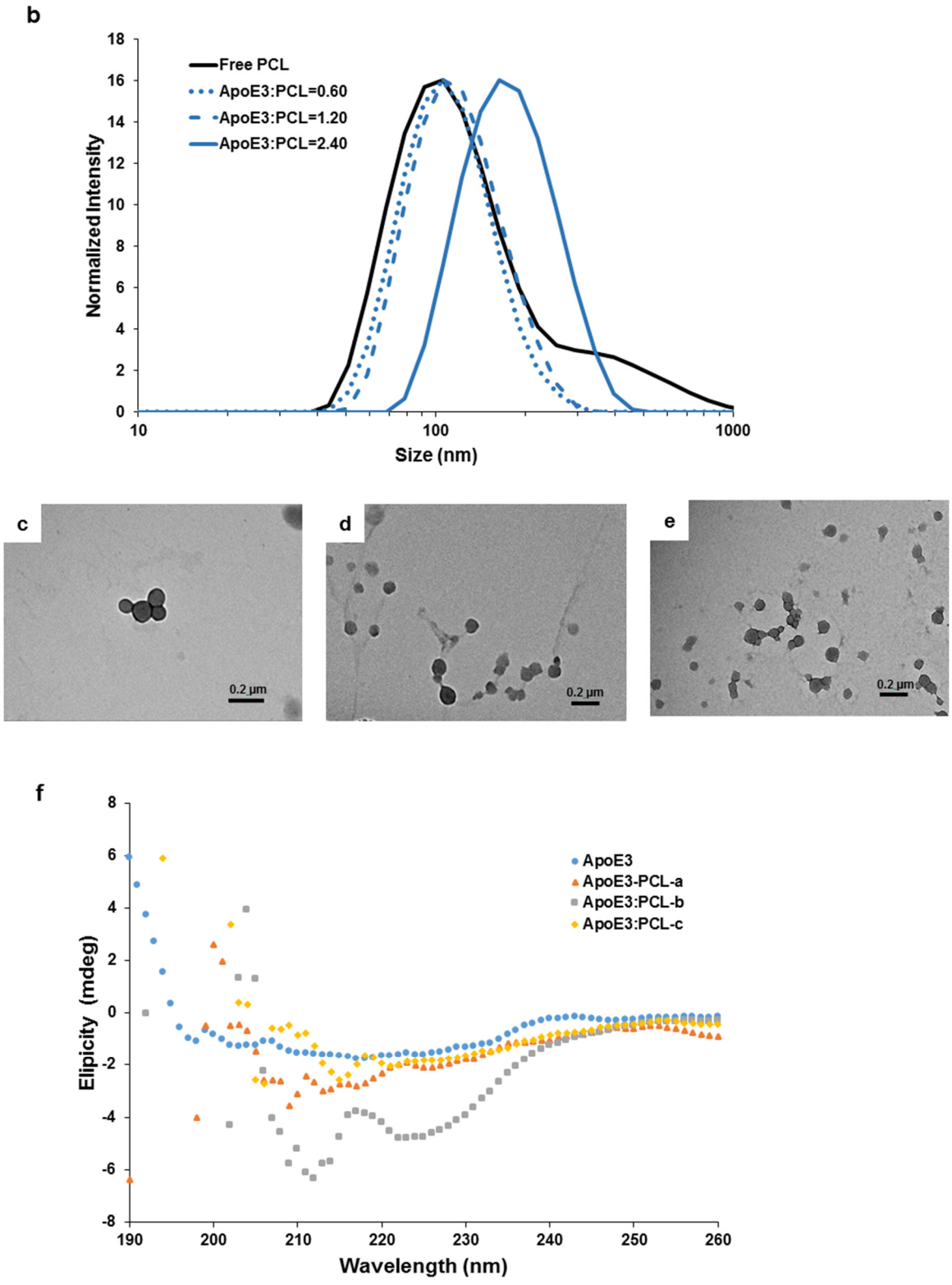
b
Free PCL
ApoE3:PCL=0.60
ApoE3:PCL=1.20
ApoE3:PCL=2.40
Normalized Intensity
Size (nm)
c
d
e
0.2 μm
f
ApoE3
ApoE3-PCL-a
ApoE3:PCL-b
ApoE3:PCL-c
Elipicity (mdeg)
Wavelength (nm)

Figure 3.4. (a) Schematic illustration of the synthesis of ApoE3-PCL-py-NPs. **(b)** DLS results of ApoE3-PCL-py-NPs with different mass ratio (M_{ApoE3}/M_{PCL-py}) of 0.60, 1.20 and 2.40. TEM images of ApoE3-PCL-py-NPs at different mass ratio, where **(c)** M_{ApoE3}/M_{PCL-py}= 0.60 **(d)** M_{ApoE3}/M_{PCL-py} = 1.20 **(e)** M_{ApoE3}/M_{PCL-py} = 2.40. **(f)** Circular dichroism of ApoE3 and ApoE3-PCL-py-NPs, ApoE3:PCL-py-a is M_{ApoE3}/M_{PCL-py} = 0.60; ApoE3:PCL-py-b is M_{ApoE3}/M_{PCL-py} = 1.20; ApoE3:PCL-py-c is M_{ApoE3}/M_{PCL-py} = 2.40. The CD spectra is not good enough to tell any conformational changes.

Table 3.3 Sizes of ApoE3-PCL-py-NPs measured by DLS (a-c) with different mass ratios of proteins to PCL-py (M_{ApoE3}/M_{PCL-py}).

System	M_{ApoE3}/M_{PCL-py}	Size (nm)	PDI	Zeta potential
Free PCL-py	-	95 ± 7	0.111	N/A
ApoE3-PCL-py-a	0.60	108 ± 6	0.173	-19.47
ApoE3-PCL-py-b	1.20	121 ± 5	0.200	-15.93
ApoE3-PCL-py-c	2.40	151 ± 21	0.154	-18.37

3.5 CELL VIABILITY ASSAY

The cytotoxic effects of P4VP and PCl-py nanoparticles were evaluated using human umbilical vein endothelial cells (HUVECs) and human mesenchymal stem cells (hMSCs), using the CellTiter-Blue cell viability assay. Both cell types were treated with ApoE3-P4VP-NPs and ApoE3-PCL-py-NPs for 24 h. As can be seen in Figure 3.5, both cell types showed high percentage of cell viability when treated with both types of nanoparticles, however it seemed like PCL-py polymer had higher cytotoxic effect to HUVECs cells. The percent viability that went higher than 100 may possibly came from media component that gave false-positive result.

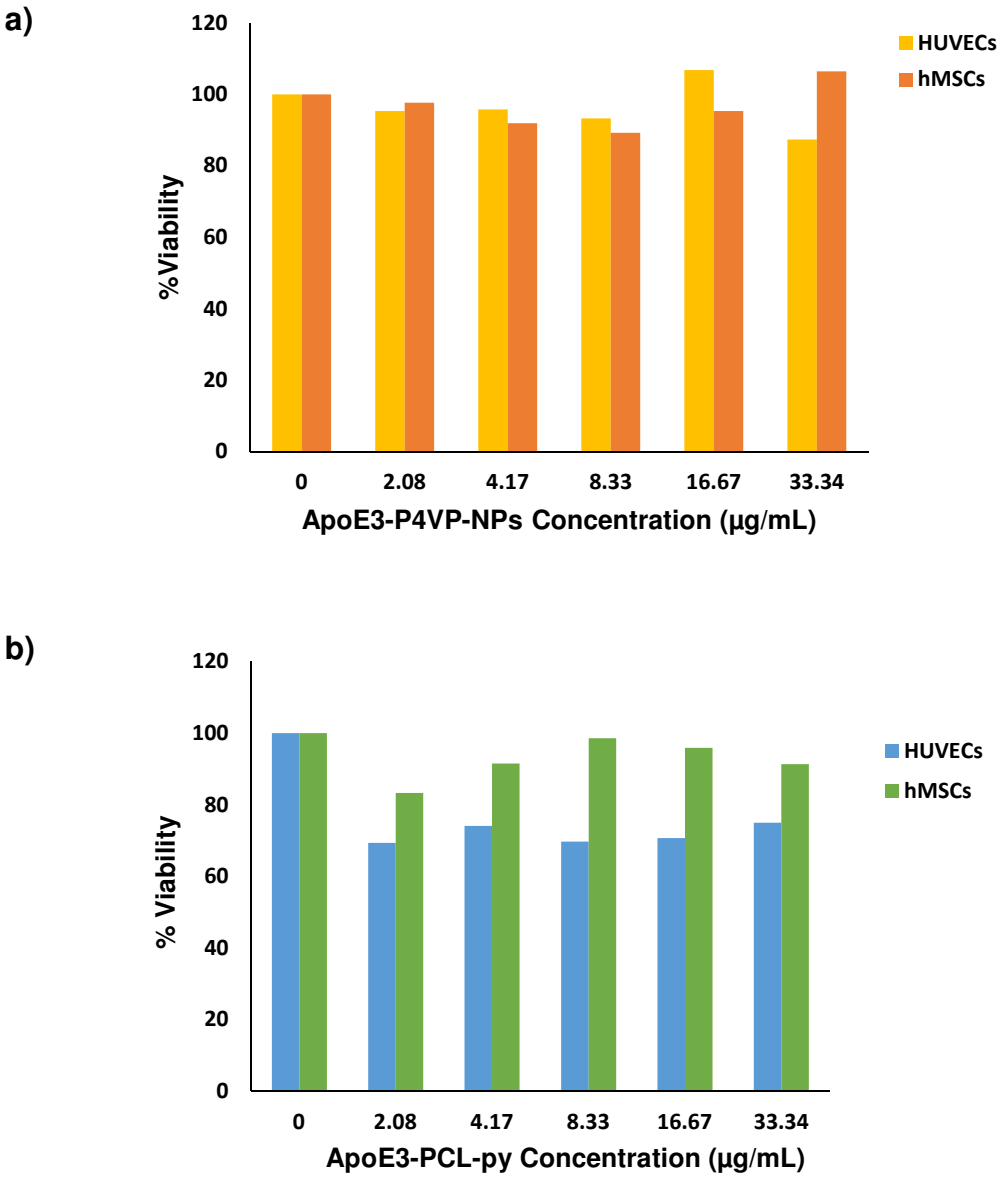

Figure 3.5. Cell viability assay of (a) ApoE3-P4VP-NPs (b) ApoE3-PCL-py-NPs treated for 24 h.

3.6 NANOPARTICLES UPTAKE IN HUVECS AND HMSCS

To investigate the *in vitro* cellular uptake of the developed nanoparticles, Fl-ApoE3-P4VP-NPs, with a mass ratio of $M_{Fl\text{-}ApoE3}/M_{P4VP}$ equals to 1.20 was chosen in this study then incubated with HUVECs, LDLR receptor (+) cells and hMSCs, LDLR receptor (-) cells for 2 and 24 h. Control samples, Fl-BSA-P4VP-NPs (negative control) which were prepared by the same manner as Fl-ApoE3-P4VP-NPs and Fl-ApoE3 solution were also incubated to both cell types for 2 and 24 h, respectively. The intracellular localization of Fl-ApoE3-P4VP-NPs was visualized using confocal laser scanning microscopy. The result of nanoparticles uptake in HUVECs cells was shown in Figure 3.6 and Figure 3.7. The blue nuclei were stained with 4'6-diamidino-2-phenylindole (DAPI) while the green fluorescent belonged to the fluorescein-ApoE3. The cellular uptake of Fl-ApoE3-P4VP-NPs can be observed within 2 h of incubation time and the cells shown a stronger fluorescence signal after 24 h (Figure 3.6). The cellular uptake of the particles was mostly found in cytoplasm, while green fluorescent signal was found mostly outside the cells when incubated with the Fl-ApoE3 solution.

When Fl-BSA-P4VP-NPs were used in the experiments, only weak fluorescence signal could be found in some HUVECs cells upon 2 h incubation. The signal was stronger upon 24 h incubation. Another controlled experiment was done in order to confirm our hypothesis that the particles were uptaken into the cells via LDLR receptor by pre-treated the cells with ApoE3 solution for 2 h, then incubated with Fl-ApoE3-P4VP-NPs for 2 and 24 h respectively. The results showed in Figure 3.6 and Figure 3.8 that only a few green fluorescent signal could be found in the cells. The result of nanoparticles uptake in hMSCs cells is shown in Figure 3.9 with the same operation as in HUVECs cells, the fluorescence

signal was very weak for all samples in both 2 and 24 h of incubation time.

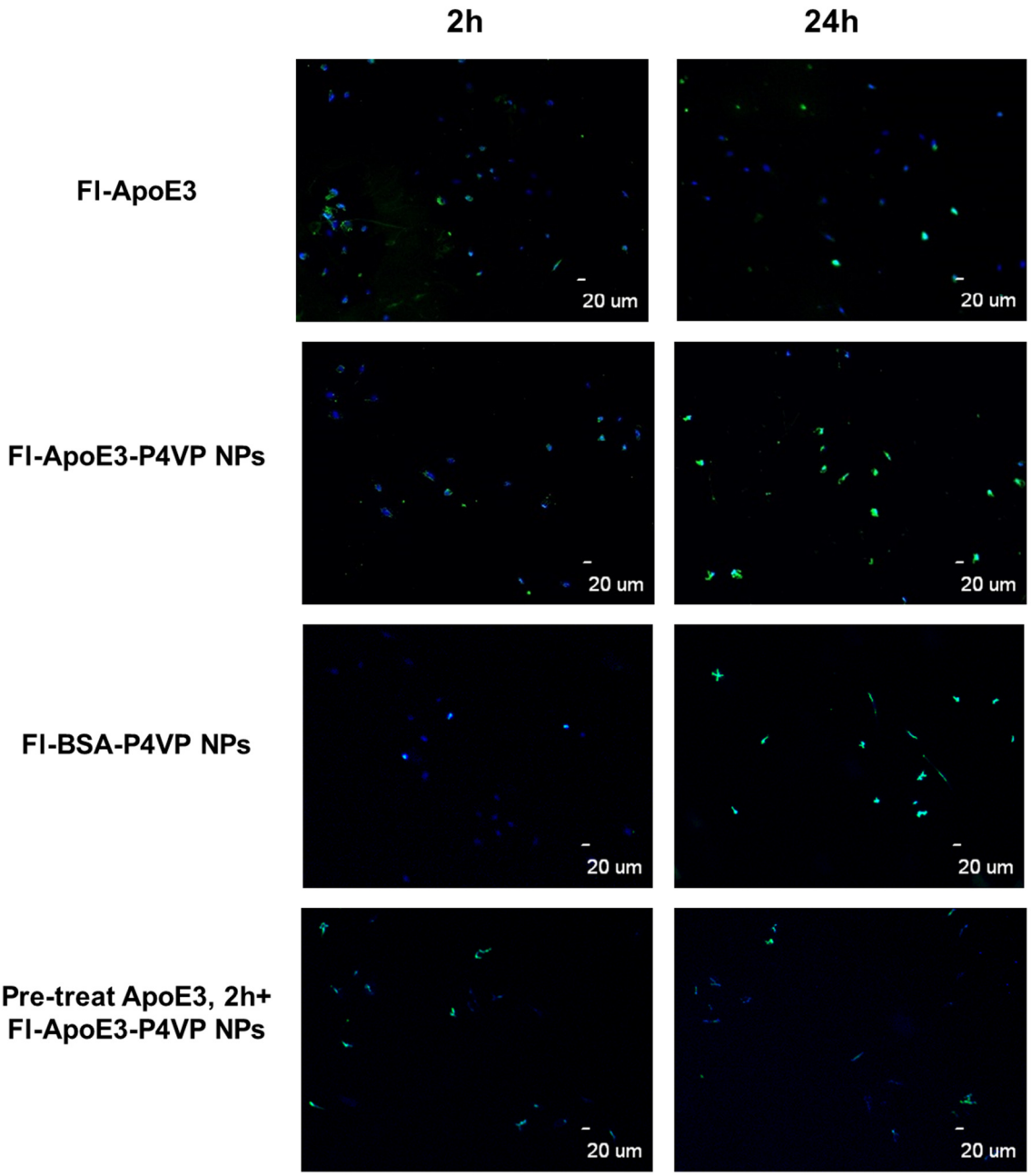

Figure 3.6. Fluorescent microscopic images of HUVECs (LDLR receptor+) cells incubated with Fl-ApoE3, Fl-ApoE3-P4VP-NPs, Fl-BSA-P4VP-NPs for 2, 24h and pre-treated with ApoE3 for 2 h follow by the incubation of Fl-ApoE3-P4VP-NPs for 2, 24 h. The blue nuclei of cells were stained with DAPI. The green fluorescence belonged to the Fl-ApoE3. The scale bars are 20 µm.

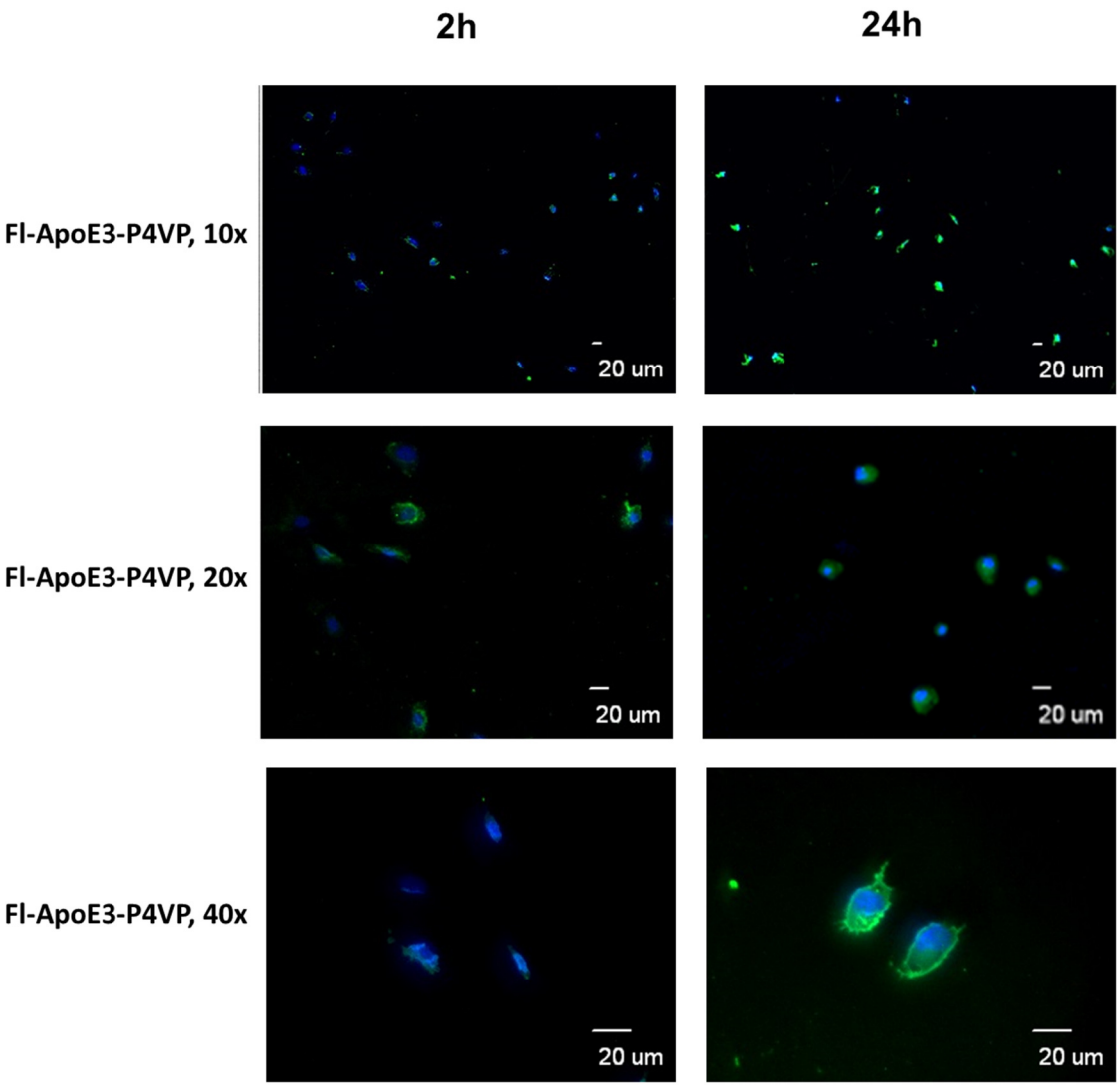

Figure 3.7. High magnification fluorescent microscopic images of HUVECs (LDLR receptor+) cells incubated with Fl-ApoE3-P4VP-NPs, for 2, 24h. The blue nuclei of cells were stained with DAPI. The green fluorescence belonged to the Fl-ApoE3. The scale bars are 20 μm.

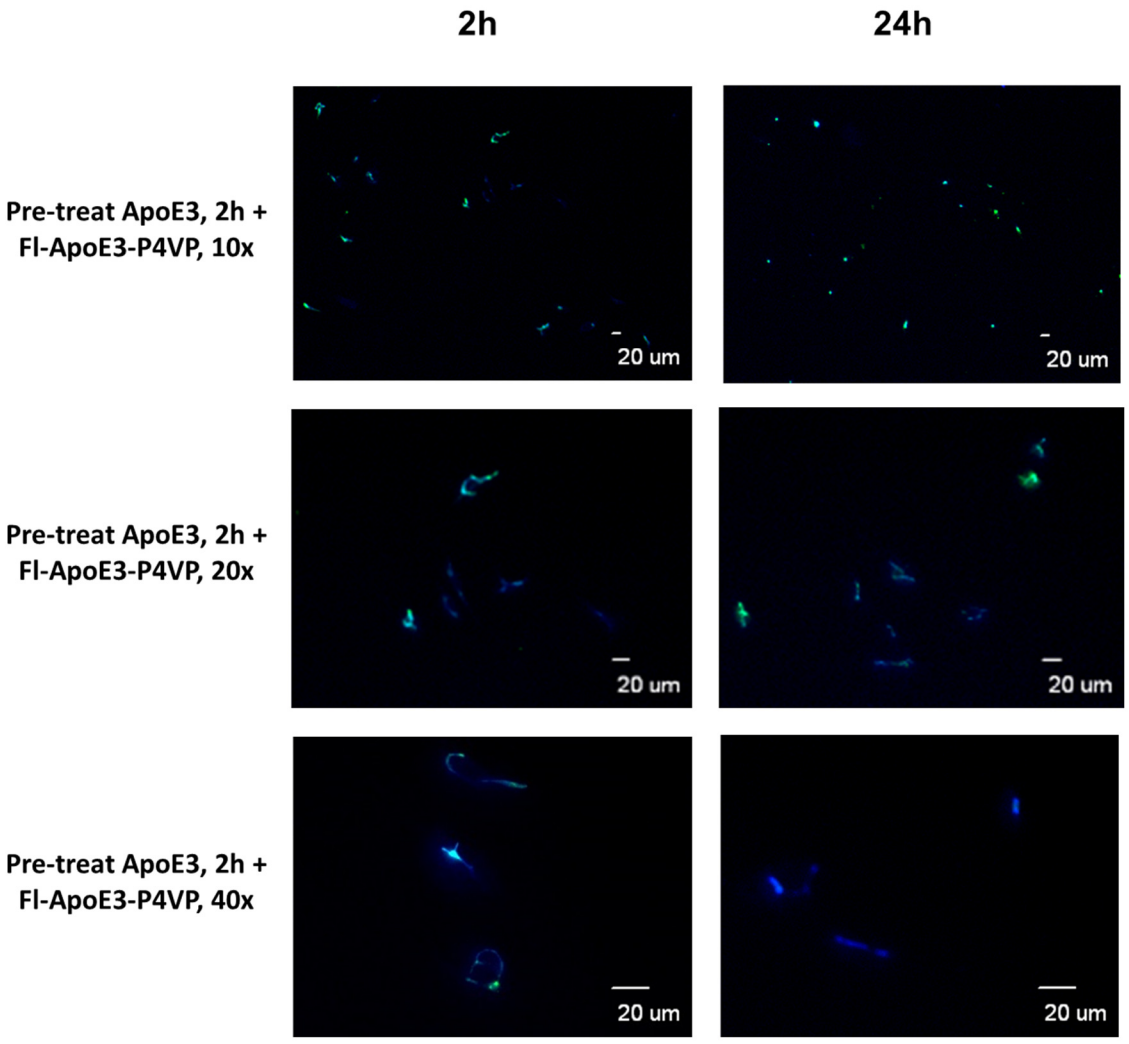

Figure 3.8. Fluorescent microscopic images of HUVECs (LDLR receptor+) cells pre-incubated with ApoE3 for 2 h, then incubated with Fl-ApoE3-P4VP-NPs for 2, 24h. The blue nuclei of cells were stained with DAPI. The green fluorescence belonged to the Fl-ApoE3. The scale bars are 20 µm.

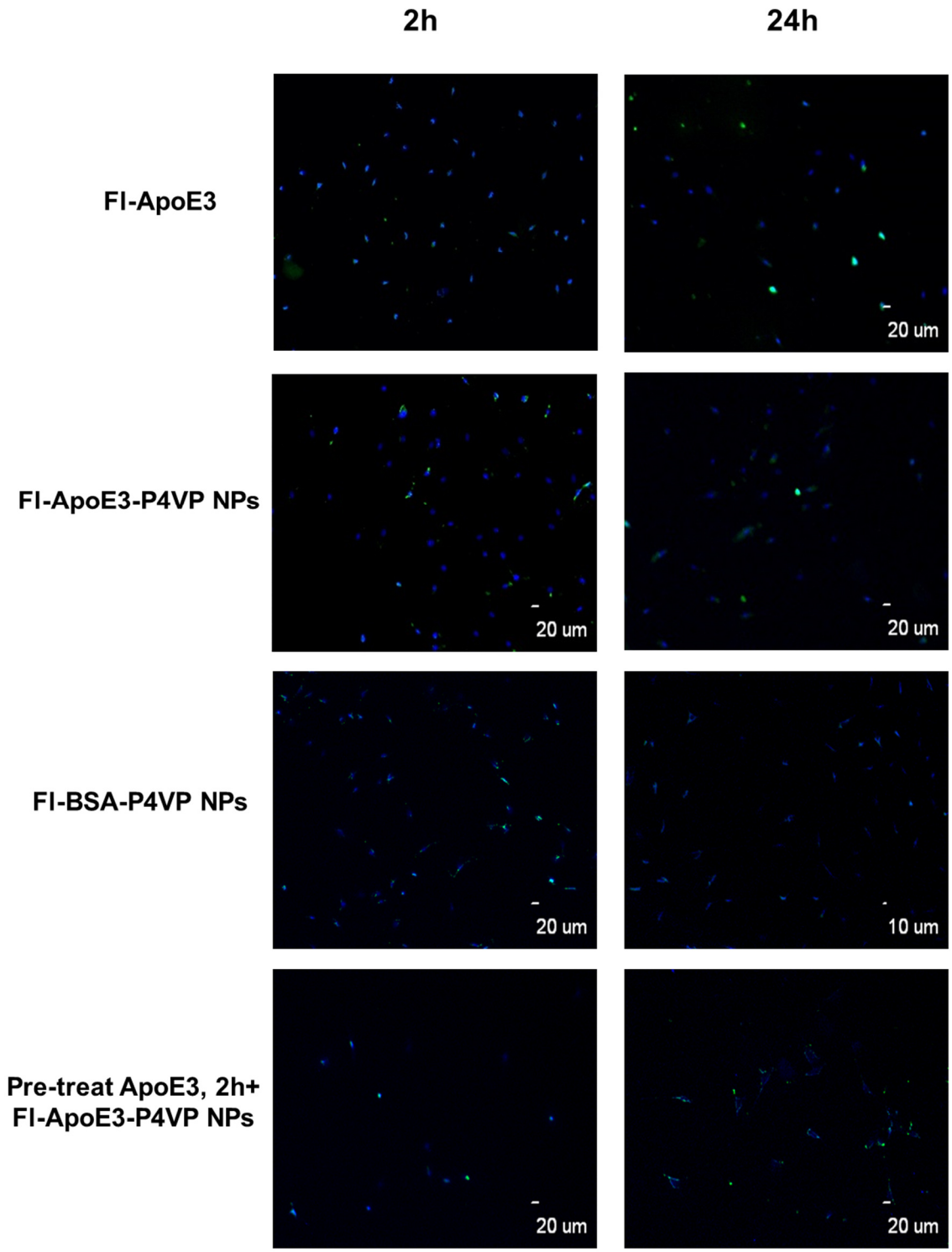

Figure 3.9. Fluorescent microscopic images of hMSCs (LDLR receptor-) cells incubated with Fl-ApoE3, Fl-ApoE3-P4VP-NPs, Fl-BSA-P4VP-NPs for 2, 24h and pre-treated with ApoE3 for 2 h follow by the incubation of Fl-ApoE3-P4VP-NPs for 2, 24 h. The blue nuclei of cells were stained with DAPI. The green fluorescence belonged to the Fl-ApoE3. The scale bars are 20 μm.

3.7 Self-assembly of Fluorescently labeled ApoE3-P4VP encapsulated Nile Red Nanoparticles (Fl-ApoE3-P4VP/NR-NPs)

For synthesis of Fl-ApoE3-P4VP/NR-NPs, a P4VP solution in ethanol was mixed with nile-red solution in ethanol in 1:1 ratio, then the solution was added dropwise in the Fl-ApoE3 solution. The particles with different mass ratio, i.e. $M_{Fl\text{-}ApoE3}/M_{P4VP/NR}$: 0.60, 1.20 and 2.40, were analyzed by DLS (Figure 3.10). The average sizes, PDI and zeta potential of the particles were shown in Table. 3.4.

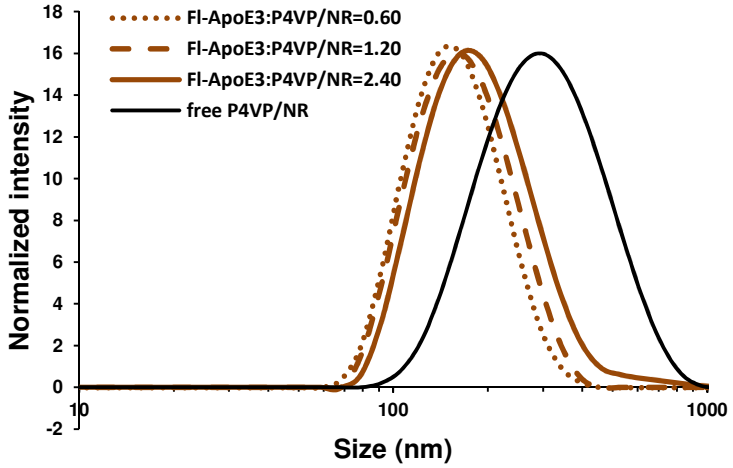

Figure 3.10. DLS results of Fl-ApoE3-P4VP/NR-NPs with different mass ratio ($M_{Fl\text{-}ApoE3}/M_{P4VP/NR}$) of 0.60, 1.20 and 2.40.

Table 3.4 Sizes of Fl-ApoE3-P4VP/NR-NPs measured by DLS (a-c) with different mass ratios of proteins to P4VP/NR ($M_{Fl\text{-}ApoE3}/M_{P4VP/NR}$).

System	$M_{Fl\text{-}ApoE3}/M_{P4VP/NR}$	Size (nm)	PDI	Zeta potential
Free P4VP/NR	-	367 ± 40	0.343	-10.25
Fl-ApoE3-P4VP/NR-a	0.60	160 ± 0.4	0.173	-0.24
Fl-ApoE3-P4VP/NR-b	1.20	176 ± 0.3	0.272	-27.73
Fl-ApoE3-P4VP/NR-c	2.40	208 ± 6	0.358	-28.03

3.8 CONCLUSION

Different types of nanoparticles were prepared in a well-defined structure with controllable size by self-assembly process. Hydrogen bonding between proteins and polymers and a fine balance of hydrophilicity and hydrophobicity of the polymers was believed as key to the assembly process. The results from cellular uptake of the developed nanoparticles studies shown the ability of ApoE3 to facilitate and specifically targeted deliver nanoparticles in BBB cell model, HUVECs cells, via LDLR receptor mediated endocytosis.

3.9 MATERIALS AND METHOD

MATERIALS

Human umbilical vein endothelial cells (HUVECs) was obtained from Dr. Melissa A. Moss (University of South Carolina, department of biomedical engineering). Dulbecco's modified Eagle's medium (DMEM) and fetal bovine serum (FBS) were purchased from VWR. Trypsin/ EDTA solution and penicillin-streptomycin (P/S) were purchased from Hyclone. F-12K Nutrient Mixture (Kaighn's Mod.) with L-glutamine was purchased from VWR. Endothelial cell growths supplement from bovine neural tissue (ECGS) and heparin sodium salt from porcine intestinal mucosa were purchased from Sigma-Aldrich. NHS-fluorescein was purchased from Pierce. P4VP (Mw 60,000) was purchased from Sigma-Aldrich. PCL-py (Mw 10,000) was synthesized by Dr. Jing Yan. Apolipoprotein E3 was purified from pre-engineered 293T-ApoE3 cells. Fluorescently labelled Apolipoprotein E3 (Fl-ApoE3) was synthesized following the process explained in chapter 2. Water was obtained from Milli-Q system (Millipore). Cell Titer Blue Reagent

and 4',6-Diamidino-2-phenylindole were purchased from VWR. Nile red was purchased from Sigma-Aldrich.

FLUORESCEIN-CONJUGATED PROTEINS

A solution of NHS-fluorescein in DMSO (50 µL; 1 mg mL^{-1}) was slowly added (1 drop/ 10 s) into a solution of protein (2 mg mL^{-1} in PBS buffer pH 7.4) at 4 ^{o}C with gently stirring. The solution mixture was incubated in dark at 4 ^{o}C for 2 h. Then, the excess NHS-fluorescein was removed by using nanosep centrifugal system with Mw cutoff 10 kDa, centrifuged at 5,000 x g for 5 mins, 2 times. The fluorescein conjugated protein was analyzed by SDS-PAGE.

A TYPICAL PROCEDURE TO SYNTHESIZE P4VP-PROTEIN STRUCTURES

A solution of P4VP (Mw 60,000 Da) in ethanol (2.0 mg mL^{-1}, 0.1 mL) was slowly added (1 drop/ 10 s) into a protein solution (0.04, 0.02, 0.01 mg mL^{-1}, diluted from 2.0 mg mL^{-1} stock solution) in water with stirring at high speed for 2 h. The mixtures were then placed under fume hood with stirring at the same speed, at room temperature, cap off, for half a day to allow ethanol to completely evaporate. Samples were analyzed by DLS, CD analysis and TEM thereafter. This method was adapted from Suthiwangcharoen *et al* [21].

A TYPICAL PROCEDURE TO SYNTHESIZE PCL-PY-PROTEIN STRUCTURES

A solution of PCL-py (Mw ~15 kDa) in dimethylformamide (DMF) (2.0 mg mL^{-1}, 0.1 mL) was slowly added (1 drop/ 10 s) into an protein solution (0.04, 0.02, 0.01 mg mL^{-1}, diluted from 2.0 mg mL^{-1} stock solution) in water with stirring at high speed for 2 h. The mixtures were then dialyzed against 4 L of 1xPBS buffer for 4 h, change buffer every

2 h in order to remove the organic solvent. Samples were analyzed by DLS, CD analysis and TEM thereafter. This method was adapted from Suthiwangcharoen *et al* [21].

CD ANALYSIS

Circular dichroism (CD) was performed on a Jasco 815 spectrophotometer using a quartz cuvette with a 2 mm path length. Scans were taken from 190 to 260 nm at a rate of 100 nm/min with a 1 mm step resolution and a 1 s response. Three scans were conducted at a constant temperature of 25 ^{o}C and the average was reported. The experiment was done with help from John Hepburn.

ENCAPSULATION OF NILE RED IN FL-APOE3-P4VP-NPS

A nile red solution in ethanol (2 mg mL^{-1}, 250 µL) was mixed with a solution of P4VP in ethanol (2 mg mL^{-1}, 250 µL). The solution mixture was then added dropwise (1 drop/ 10 s) into the Fl-ApoE3 protein solution (0.04, 0.02, 0.01 mg/mL, diluted from 2.0 mg mL^{-1} stock solution) in water with stirring at high speed for 2 h. The mixtures were then placed under fume hood (in dark) with stirring at the same speed, at room temperature, cap off, for half a day to allow ethanol to completely evaporate. The excess nile red was removed by centrifugation at 4000 x g for 7 min. The remainder supernatant was then analyzed by DLS. This method was adapted from unpublished data of Suthiwangcharoen, N.

CELLULAR UPTAKE OF NANOPARTICLES

Human umbilical-vein endothelial cells (HUVECs) which was obtained from Dr. Melissa A. Moss (University of South Carolina, Department of biomedical engineering) were maintained in 1:1 F12K:Dulbecco's Modified Eagle Medium (DMEM) media supplemented with 10% fetal bovine serum (FBS), 1% penicillin/ streptomycin (P/S), 50 mg of heparin and 15 mg of endothelial cell growths (ECGS) and were used at passage 6-10. Human mesenchymal stem cells (hMSCs) were maintained in DMEM medium supplemented with 10% fetal bovine serum (FBS), 1% penicillin/ streptomycin (P/S) and were used at passage 6-10. Cells were grown at 37 ^{o}C with 5% CO_2. A confluent 75 cm^2 flask of cells was dispersed using 0.05% trypsin/EDTA solution. Cells were resuspended in 1% FBS media and plated in 6-well tissue culture plate at the density of 1.5 x 10^4 cell/mL, 48 h prior experiment. Cells were then incubated with the different samples with ratio of treatment : 1% FBS medium = 1:1, for 2 and 24 h. After incubation, cells were washed with PBS and fixed with 4% formaldehyde and washed several times with PBS. Later, cells were stained with DAPI reagent for 10 min followed by several washes with PBS. Finally, cells were mounted on a microscope slide and visualized using a confocal microscope.

CELL TITER BLUE ASSAY

Cell viability was determined using the conventional CellTiter-Blue assay. Each cell was seeded on a 96-well plate at a density of 1.0 x 10^5 cell/mL, 100 µL/well and incubated at 37 ^{o}C, 5% CO_2 for 24 h. Medium containing various concentration of samples was added to each well, 100 µL/well. After 24 h of incubation, CellTiter-Blue solution (20

μL) was added to each well and incubated for another 4 h. The fluorescence was measured on a Spectra Max Gemini EM spectrophotometer with an excitation wavelength of 560 nm and an emission wavelength of 590 nm.

REFERENCES

1. Michaelis, K., Hoffmann, M.M., Dreis, S., Herbert, E., Alyautdin, R.N., Michaelis, M., Kreuter, J., & Langer, K. (2006). Covalent linkage of apolipoprotein e to albumin nanoparticles strongly enhances drug transport into the brain. *Journal of Pharmacology and Experimental Therapeutics. 317*(3). 1246-1253.

2. Wohlfart, S., Gelperina, S., & Kreuter, J. (2012). Transport of drugs across the blood brain barrier by nanoparticles. *Journal of Controlled Release. 161*(2). 264-273.

3. Georgieva, J.V., Hoekstra, D., & Zuhorn, I.S. (2014). Smuggling Drugs into the Brain: An Overview of Ligands Targeting Transcytosis for Drug Delivery across the Blood-Brain Barrier. *Pharmaceutics. 6*(4). 557-583.

4. Gelperina, S., Maksimenko, O., Khalansky, A., Vanchugova, L., Shipulo, E., Abbasova, K., Berdiev, R., Wohlfart, S., Chepurnova, N., & Kreuter, J. (2010). Drug delivery to the brain using surfactant-coated poly(lactide-co-glycolide) nanoparticles: Influence of the formulation parameters. *European Journal of Pharmaceutics and Biopharmaceutics. 74*(2). 157-163.

5. Ulbrich, K., Knobloch, T., & Kreuter, J. (2011). Targeting the insulin receptor: nanoparticles for drug delivery across the blood-brain barrier (BBB). *Journal of Drug Targeting. 19*(2): p. 125-132.

6. Upadhyay, R.K. (2014). Drug delivery systems, CNS protection, and the blood brain barrier. *BioMed Research International. 2014*: ID 869269.

7. Kreuter, J., Alyautdin, R.N., Kharkevich, D.A., & Ivanov, A.A. (1995). Passage of peptides through the blood-brain barrier with colloidal polymer particles (nanoparticles). *Brain Research. 674*(1). 171-174.

8. Alyautdin, R.N., Petrov, V.E., Langer, K., Berthold, A., Kharkevich, D.A., Kreuter, J. (1997). Delivery of loperamide across the blood-brain barrier with polysorbate 80-coated polybutylcyanoacrylate nanoparticles. *Pharmaceutical Research. 14*(3). 325-328.

9. Alyautdin, R.N., Tezikov, E.B., Ramge, P., Kharkevich, D.A., Begley, D.J., & Kreuter, J. (1998). Significant entry of tubocurarine into the brain of rats by adsorption to polysorbate 80-coated polybutylcyanoacrylate nanoparticles: an in situ brain perfusion study. *Journal of Microencapsulation: Micro and Nano Carriers. 15*(1). 67-74.

10. Steiniger, S.C., Kreuter, J., Khalansky, A.S., Skidan, I.N., Bobruskin, A.I., Smirnova, Z.S., Severin, S.E., Uhl, R., Kock, M., Geiger, K.D., & Gelperina, S. E. (2004). Chemotherapy of glioblastoma in rats using doxorubicin-loaded nanoparticles. *International Journal of Cancer. 109*(5). 759-767.

11. Olivier, J.C., Fenart, L., Chauvet, R., Pariat, C., Cecchelli, R., & Couet, W. (1999). Indirect evidence that drug brain targeting using polysorbate 80-coated polybutylcyanoacrylate nanoparticles is related to toxicity. *Pharmaceutical Research. 16*(12). 1836-1842.

12. Kreuter, J., Ramge, P., Petrov, V., Hamm, S., Gelperina, S.E., Engelhardt, B., Alyautdin, R., Von, B.H., & Begley, D.J. (2003). Direct evidence that polysorbate-80-coated poly(butylcyanoacrylate) nanoparticles deliver drugs to the CNS via specific mechanisms requiring prior binding of drug to the nanoparticles. *Pharmaceutical Research. 20*(3). 409-416.

13. Alyaudtin, R.N., Reichel, A., Löbenberg, R., Ramge, P., Kreuter, J., & Begley, D.J. (2001). Interaction of poly(butylcyanoacrylate) nanoparticles with the blood-brain barrier in vivo and in vitro. *Journal of Drug Targeting. 9*(3). 209-221.

14. Luck, M., Schröder, W., Harnisch, S., Thode, K., Blunk, T., Paulke, B.R., Kresse, M., & Müller, R.H. (1997). Identification of plasma proteins facilitated by enrichment on particulate surfaces: analysis by two-dimensional electrophoresis and N-terminal microsequencing. *Electrophoresis. 18*(15). 2961-2967.

15. Kreuter, J., Shamenkov, D., Petrov, V., Ramge, P., Cychutek, K., Koch, B.C., & Alyautdin, R. (2002). Apolipoprotein-mediated transport of nanoparticle-bound drugs across the blood-brain barrier. *Journal of Drug Targeting. 10*(4). 317-325.

16. Goppert, T.M., & Muller, R.H. (2005). Polysorbate-stabilized solid lipid nanoparticles as colloidal carriers for intravenous targeting of drugs to the brain: comparison of plasma protein adsorption patterns. *Journal of Drug Targeting*. *13*(3). 179-187.

17. Wilson, B., Samanta, M.K., Santhi, K., Kumar, K.P., Paramakrishnan, N., & Suresh, B. (2008). Targeted delivery of tacrine into the brain with polysorbate 80-coated poly(n-butylcyanoacrylate) nanoparticles. *European Journal of Pharmaceutics and Biopharmaceutics*. *70*(1). 75-84.

18. Zensi, A., Begley, D., Pontikis, C., Legros, C., Mihoreanu, L., Wagner, S., Büchel, C., Von, B.H., & Kreuter, J. (2009). Albumin nanoparticles targeted with Apo E enter the CNS by transcytosis and are delivered to neurones. *Journal of Control Release. 137*(1). 78-86.

19. Kreuter, J., Hekmatara, T., Dreis, S., Vogel, T., Gelperina, S., & Langer, K. (2007). Covalent attachment of apolipoprotein A-I and apolipoprotein B-100 to albumin nanoparticles enables drug transport into the brain. *Journal of Control Release. 118*(1). 54-58.

20. Zensi, A., Begley, D., Pontikis, C., Legros, C., Mihoreanu, L., Büchel, C., & Kreuter, J. (2010). Human serum albumin nanoparticles modified with apolipoprotein A-I cross the blood-brain barrier and enter the rodent brain. *Journal of Drug Targeting*. *18*(10). 842-848.

21. Suthiwangcharoen, N., Li, T., Wu, L., Reno, H.B., Thompson, P., & Wang, Q. (2014). Facile co-assembly process to generate core-shell nanoparticles with functional protein corona. *Biomacromolecules. 15*(3). 948-956.

22. Russell, J.T., Lin, Y., Böker, A., Su, L., Carl, P., Zettl, H., He, J., Sill, K., Tangirala, R., Emrick, T., Littrell, K., Thiyagarajan, P., Cookson, D., Fery, A.,Wang, Q., and Russell, T.P. (2005). Self-assembly and cross-linking of bionanoparticles at liquid-liquid interfaces. *Angewandte Chemie International Edition in English. 44*(16). 2420-2426.

23. Niu, Z., He, J., Russell, T.P., & Wang, Q. (2010). Synthesis of nano/microstructures at fluid interfaces. *Angewandte Chemie International Edition in English. 49*(52). 10052-10066.

24. Li, T., Wu, L., Suthiwangcharoen, N., Bruckman, M.A., Cash, D., Hudson, J.S., Ghoshroyc, S., & Wang, Q. (2009). Controlled assembly of rodlike viruses with polymers. *Chemical Communications. 2009*(20). 2869-2871.

25. Li, T., Niu, Z., Emrick, T., Russell, T.P., & Wang, Q. (2008). Core/shell biocomposites from the hierarchical assembly of bionanoparticles and polymer. *Small. 4*(10). 1624-1629.

26. Clement, C.V., Barbier, A., Dergunov, A.D., Visvikis, A., Siest, G., Desmadril, M., Takahashi, M., Aggerbeck, L.P. (2006). The structure of human apolipoprotein E2, E3 and E4 in solution. 2. Multidomain organization correlates with the stability of apoE structure. *Biophysical Chemistry. 119*(2). 170-185.